



CFD Simulations of the Supersonic Inflatable Aerodynamic Decelerator (SIAD) Ballistic Range Tests

Joseph Brock

AMA Inc., Moffett Field, CA

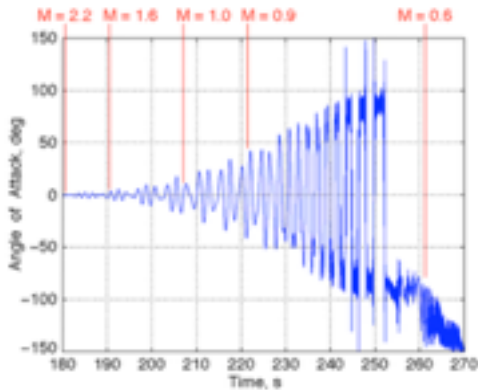
Eric Stern, and Michael Wilder

NASA Ames Research Center, Moffett Field, CA

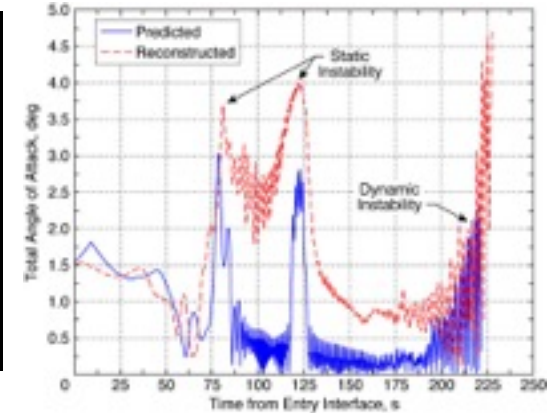
Blunt Body Dynamic Stability



Genesis Sample Return Capsule (Desai, 2008)



Mars Phoenix Lander (Desai, 2011)

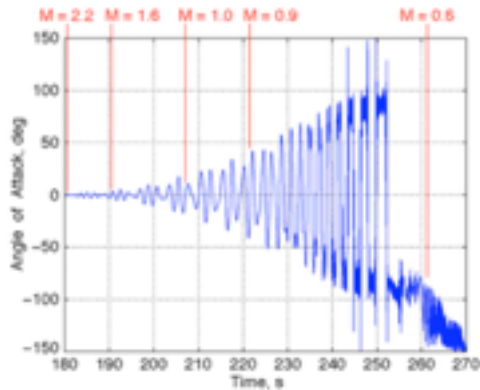


- Blunt-body capsules very effective at reducing heating to the surface
 - Dynamic instabilities often arise at low-supersonic and transonic Mach numbers
 - Dynamic stability characterized exclusively through experiment — forced-, free-oscillations, and ballistic range — however each have drawbacks resulting in uncertain predictions
 - ▶ In all cases, flight similitude parameters are difficult to achieve
- CFD an integral part of *static* aerodynamic characterization and design.
- Would be desirable to have similar capability for *dynamic* aerodynamics

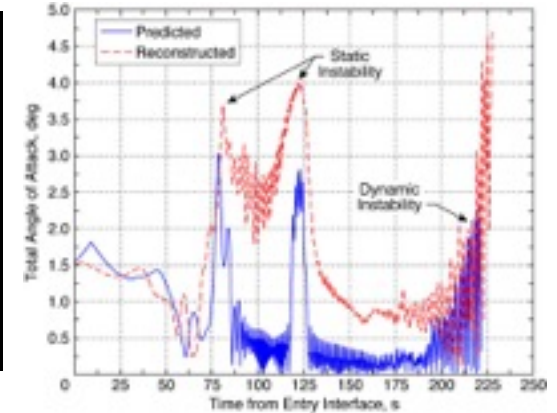
Blunt Body Dynamic Stability



Genesis Sample Return Capsule (Desai, 2008)



Mars Phoenix Lander (Desai, 2011)

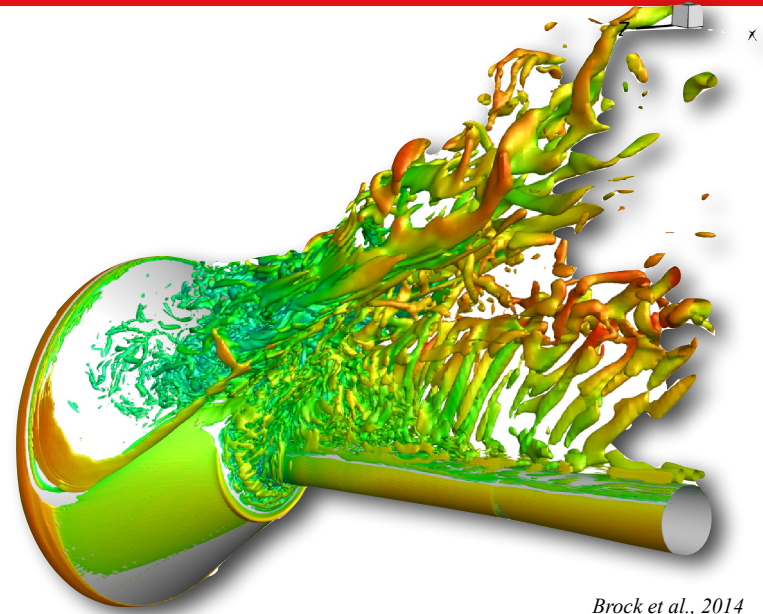


- Blunt-body capsules very effective at reducing heating to the surface
 - Dynamic instabilities often arise at low-supersonic and transonic Mach numbers
 - Dynamic stability characterized exclusively through experiment — forced-, free-oscillations, and ballistic range — however each have drawbacks resulting in uncertain predictions
 - ▶ In all cases, flight similitude parameters are difficult to achieve
- CFD an integral part of *static* aerodynamic characterization and design.
- Would be desirable to have similar capability for *dynamic* aerodynamics

US3D Dynamic Solver

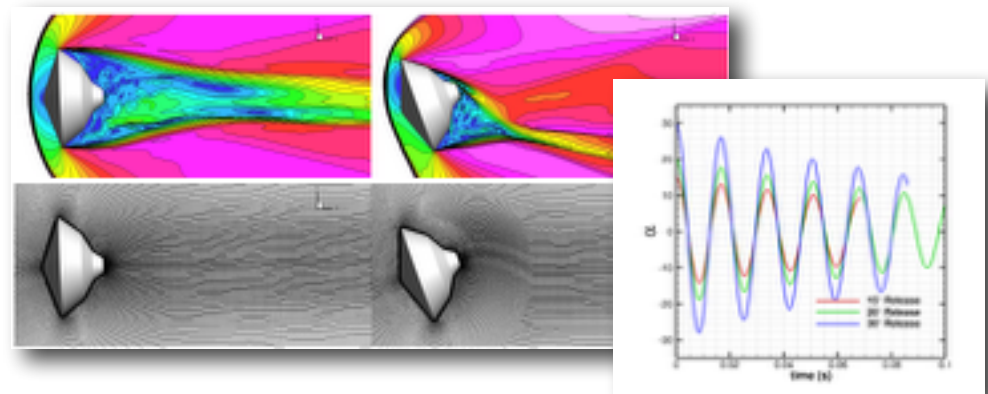


- Murman performed dynamic CFD using OVERFLOW(2009)
- Unsteady wake dynamics considered strong influence on dynamic stability
- Low-dissipation numerical schemes in US3D have been shown to provide greater resolution of wake flows
- Stern *et al.* demonstrated proof-of-concept for US3D dynamic solver simulating an MSL ballistic range



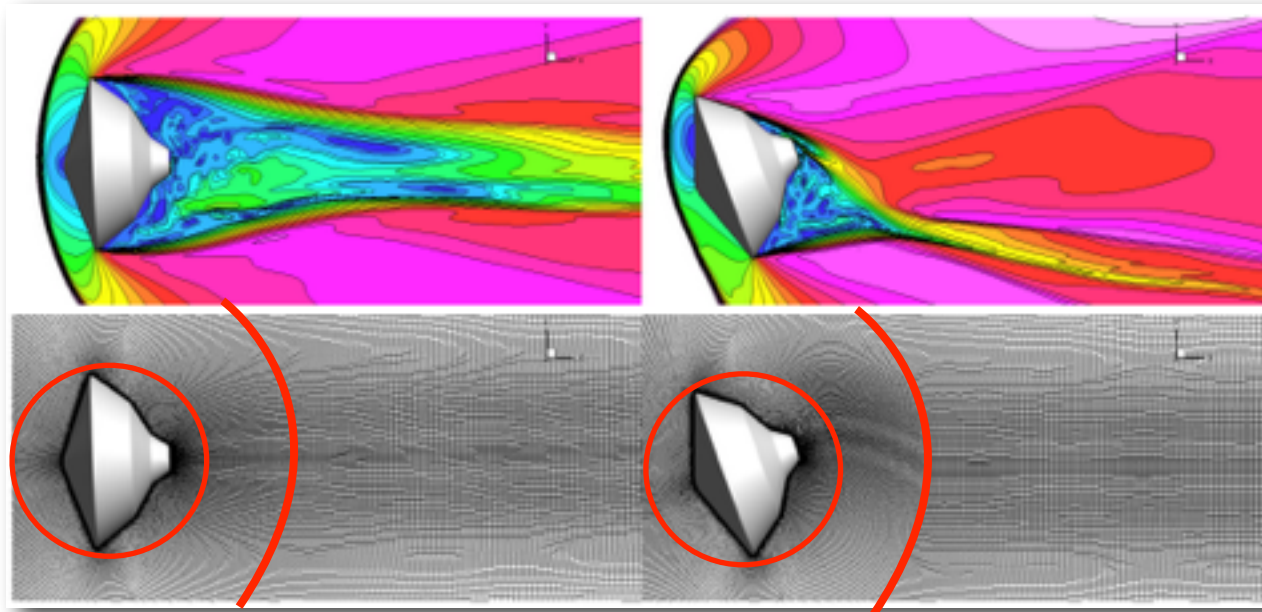
Brock *et al.*, 2014

Current work seeks to begin to validate this approach in supersonic regime through the comparison to experimental data from ballistic range



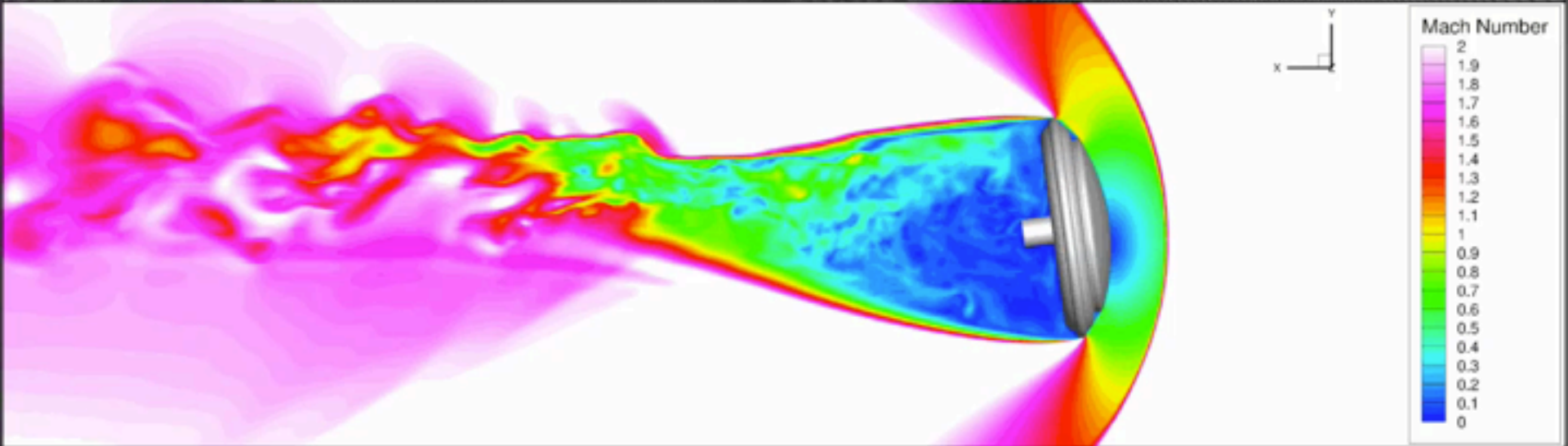
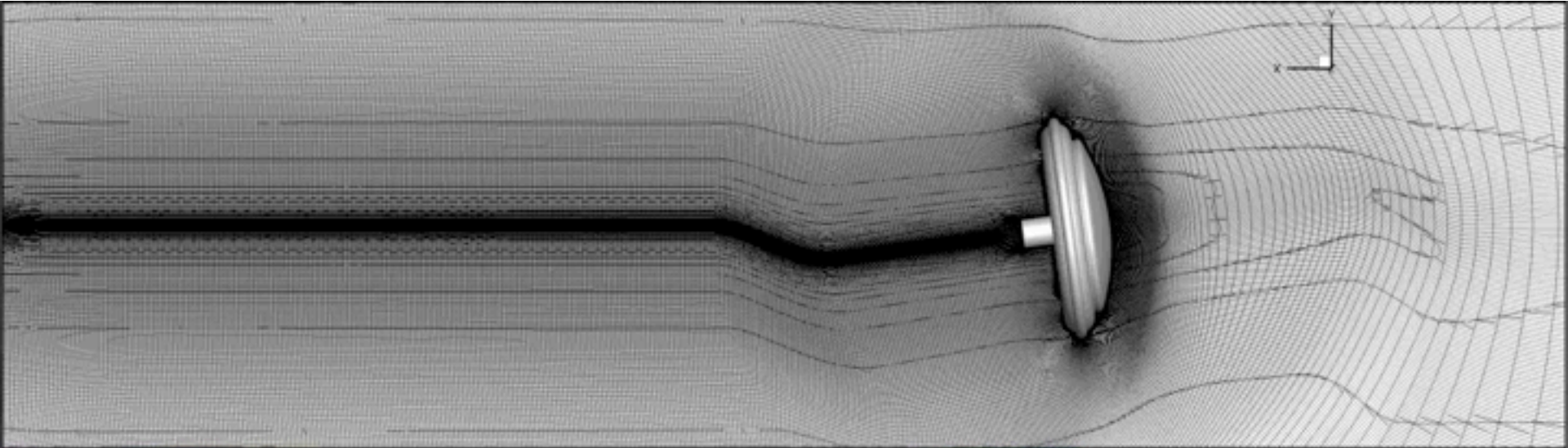
Stern *et al.*, 2013

US3D Dynamic Solver

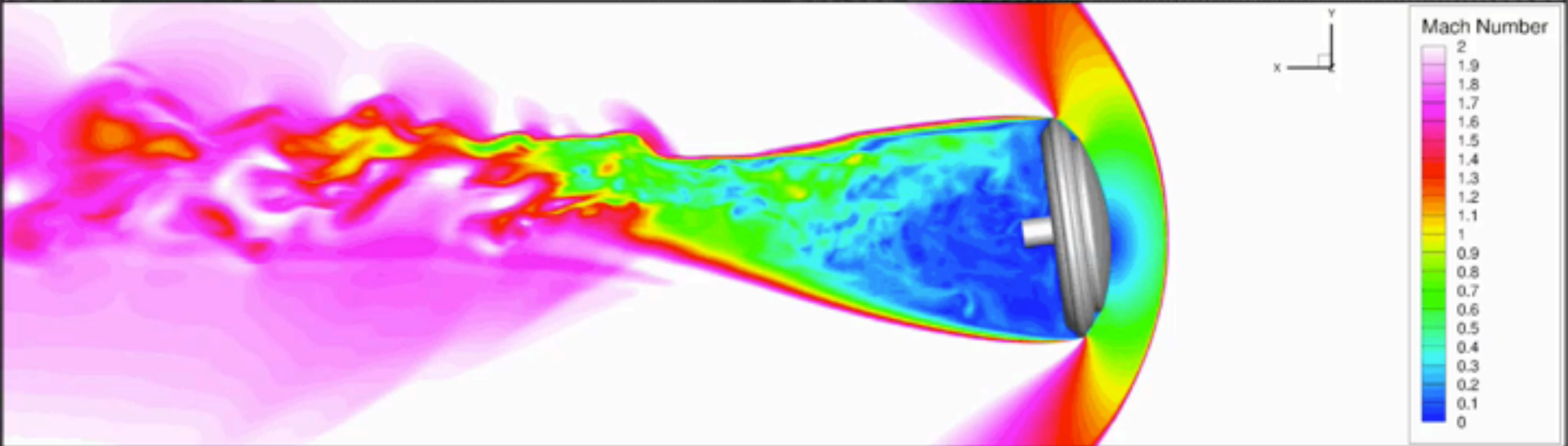
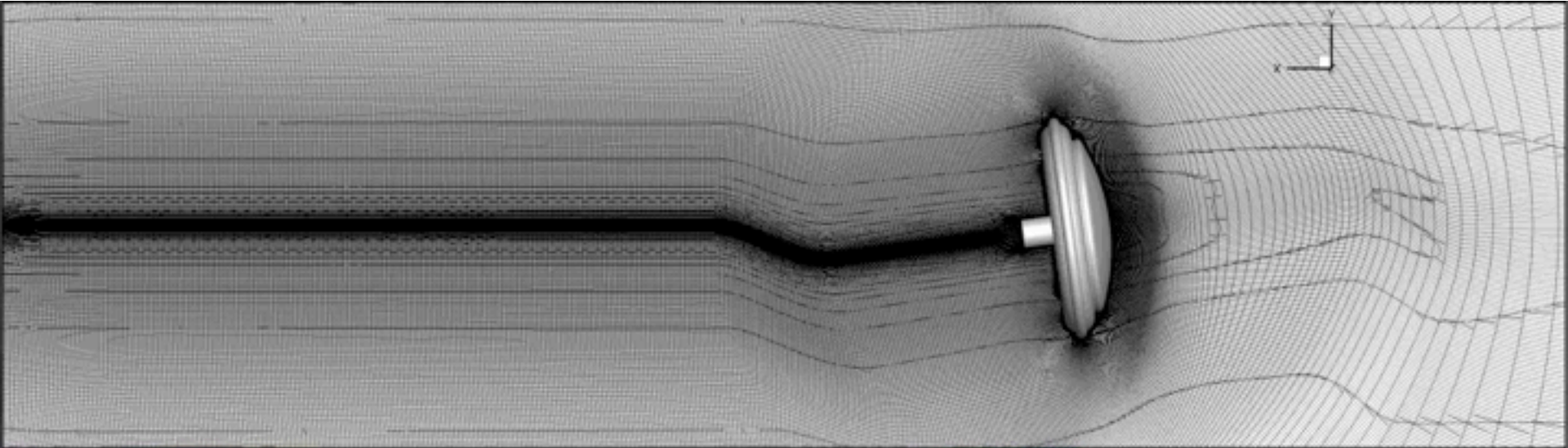


- US3D requires body-fitted mesh
- Mesh deformation employed to model 3-DOF (pitch, yaw, roll) motion
 - Inner mesh undergoes rigid body rotation with vehicle
 - Intermediate region blends inner rigid body rotating mesh to outer static region by interpolating node displacements
- Frame velocity applied to discrete governing equations when translation dynamics (i.e. acceleration, deceleration) are required

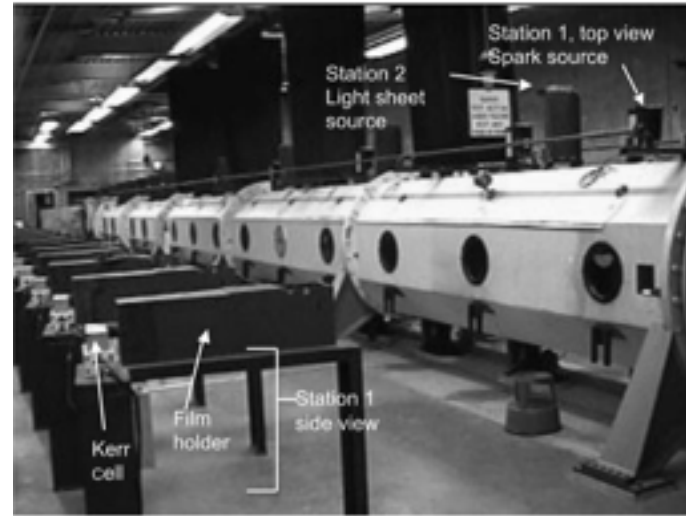
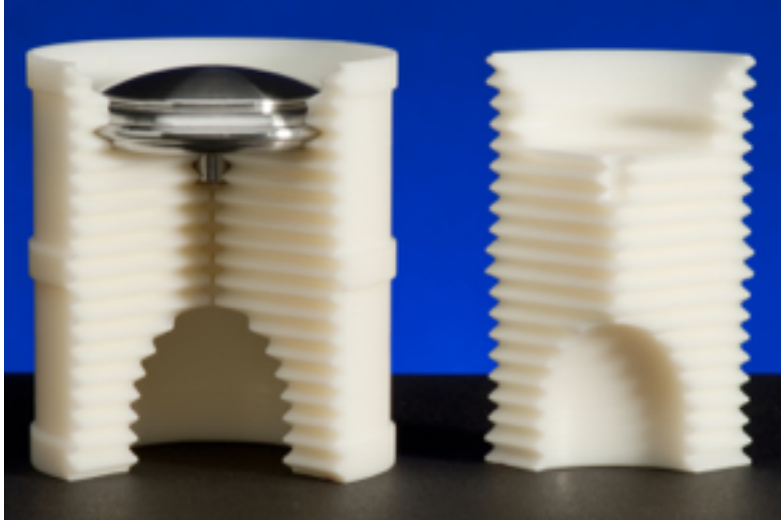
Free-Flight CFD Modeling



Free-Flight CFD Modeling



Chosen Test Conditions



- In 2013 and 2014 the Low Density Supersonic Decelerator (LDSD) project conducted the Supersonic Flight Dynamics Test (SFDT) to test the Supersonic Inflatable Aerodynamic Decelerator (SIAD)
- Ballistic range tests were conducted in the Hypervelocity Free-Flight Aerodynamics Facility (HFFAF) at NASA's Ames Research Center (ARC)
- Test series for the deployed configuration consisted of 37 shots with Mach number range 2.03 to 3.85
 - Simulations have been performed for five conditions

Chosen Test Conditions



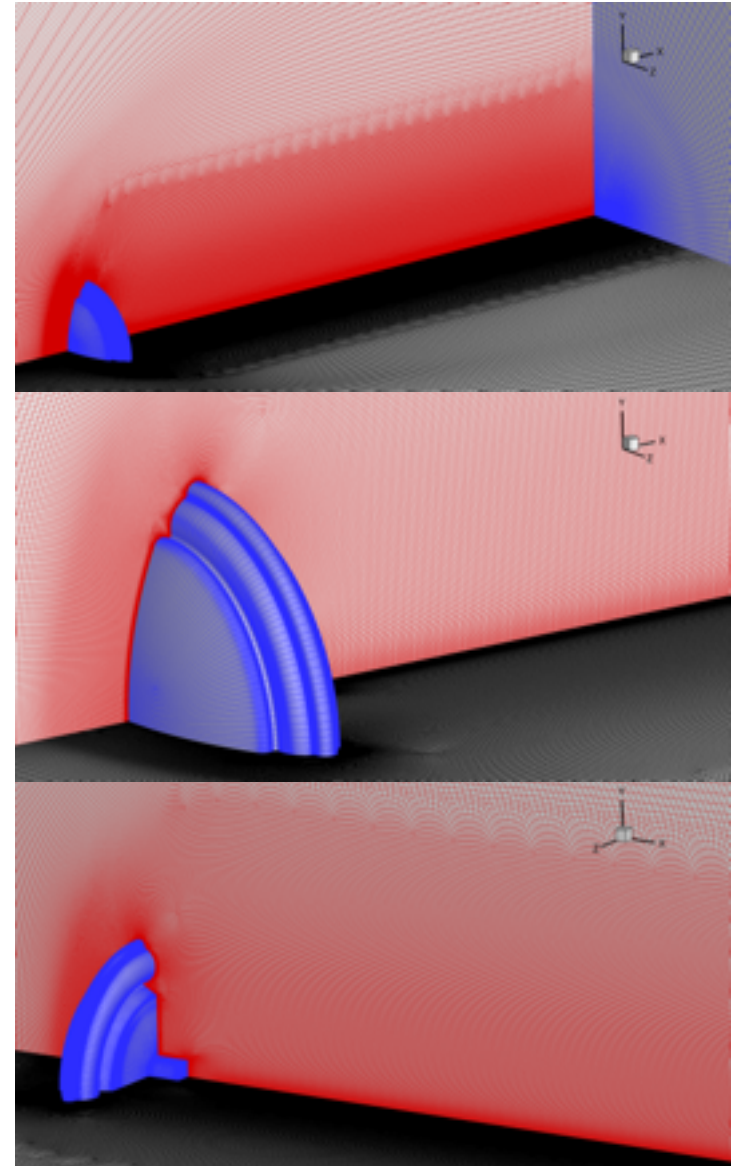
Shot	d (cm)	Mass (g)	X_{CG}/d (from nose)	I_{xx} (g-cm ²)	I_{yy} (g-cm ²)	I_{zz} (g-cm ²)	Mach	Pressure (mm Hg)	Temperature (K)
2623	3.551	45.9336	0.161	55.59	30.18	30.20	2.03	169.4	292.85
2638	3.552	45.9288	0.160	55.13	30.10	30.09	3.78	149.0	294.15
2642	3.555	45.7620	0.159	55.06	30.04	30.05	2.91	161.5	293.15
2643	3.558	45.8569	0.159	55.09	30.06	30.05	3.31	155.0	294.35
2648	3.557	45.8553	0.159	55.18	30.07	30.07	3.49	155.0	292.15

- In 2013 and 2014 the Low Density Supersonic Decelerator (LDSD) project conducted the Supersonic Flight Dynamics Test (SFDT) to test the Supersonic Inflatable Aerodynamic Decelerator (SIAD)
- Ballistic range tests were conducted in the Hypervelocity Free-Flight Aerodynamics Facility (HFFAF) at NASA's Ames Research Center (ARC)
- Test series for the deployed configuration consisted of 37 shots with Mach number range 2.03 to 3.85
 - Simulations have been performed for five conditions

Computational Mesh



- The computational mesh was generated using commercial software GridPro [8]
 - Mesh contains ~22 million hexahedral elements
 - Near wall grid spacing is ~0.1 microns ensuring y^+ values of less than 1
- Complex nested refinement allows for high grid resolution to be localized to wake region and coarsened away from regions of interest
 - The local cell size in wake is roughly 0.4mm
- Flow initialization (with static orientation) is obtained with 256 cores
 - Roughly 5 hours to fully initiate flow
- Dynamic simulations use a global time step of $1e-7$ seconds
 - Time step chosen to restrict local CFL in wake region to be of unity or less in separated region
 - Full free-flight trajectory obtained in 200 hours (~8 days using 256 cores)





Flow Initialization

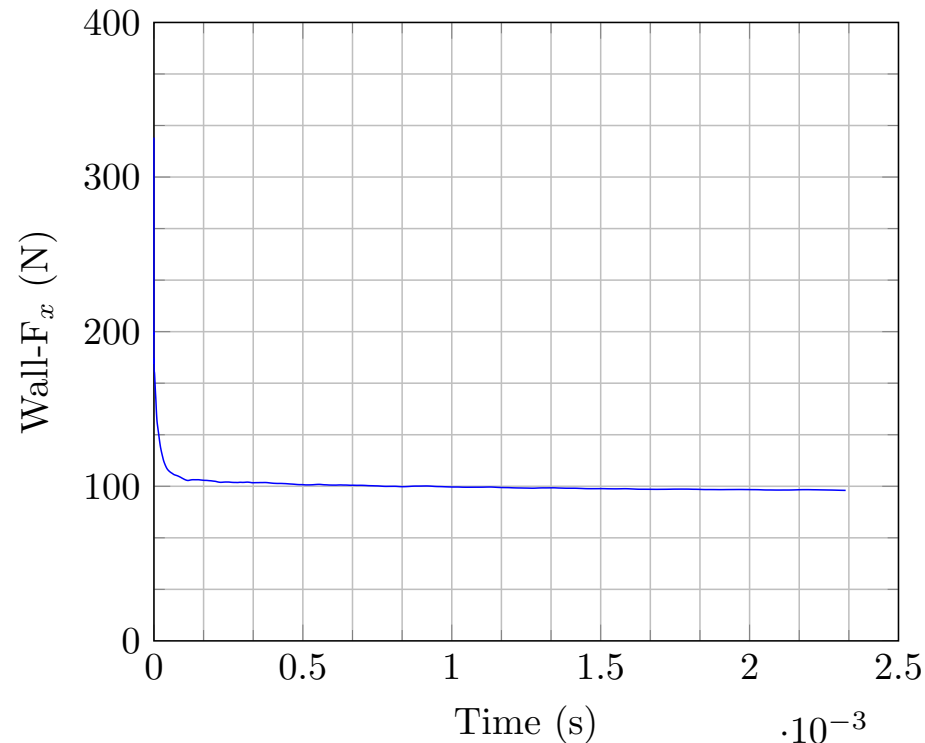


- The simulation is initialized at static orientation corresponding to first experimental observation port
- Time integration is performed using second-order Data Parallel Line Relaxation (DPLR)
- Spatial integration is performed using the second-order modified Steger-Warming flux for initialization
 - Second order low-dissipation flux scheme is used for dynamic simulations
- Turbulence is modeled using the one-equation Spalart-Allmaras eddy-viscosity model in a wall modeled Large Eddy Simulation (LES) formulation, Detached Eddy Simulation (DES97)
- Static simulations are run until wall forces converge to steady state values
- The SIAD geometry encourages separation at peak diameter, producing extensive separated region in after body region

Shot	Mach
2623	2.03



Wall- F_x vs Time



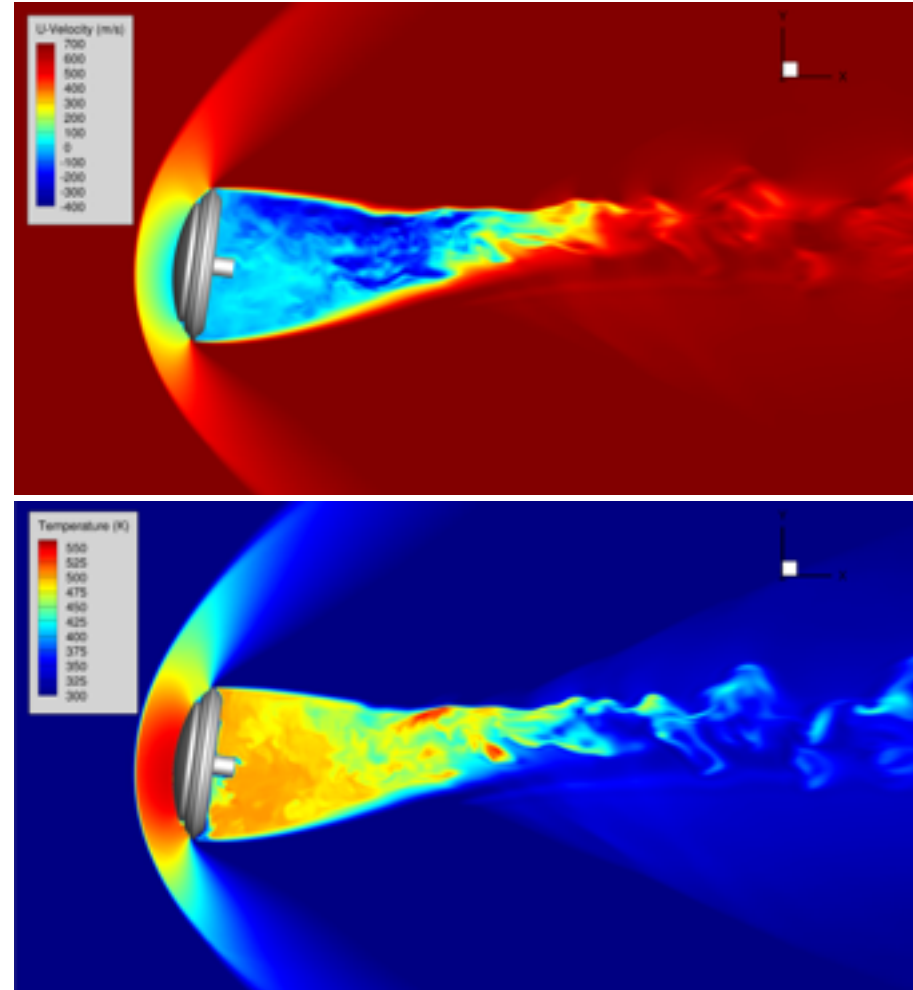


Flow Initialization



Shot	Mach
2623	2.03

- The simulation is initialized at static orientation corresponding to first experimental observation port
- Time integration is performed using second-order Data Parallel Line Relaxation (DPLR)
- Spatial integration is performed using the second-order modified Steger-Warming flux for initialization
 - Second order low-dissipation flux scheme is used for dynamic simulations
- Turbulence is modeled using the one-equation Spalart-Allmaras eddy-viscosity model in a wall modeled Large Eddy Simulation (LES) formulation, Detached Eddy Simulation (DES97)
- Static simulations are run until wall forces converge to steady state values
- The SIAD geometry encourages separation at peak diameter, producing extensive separated region in after body region

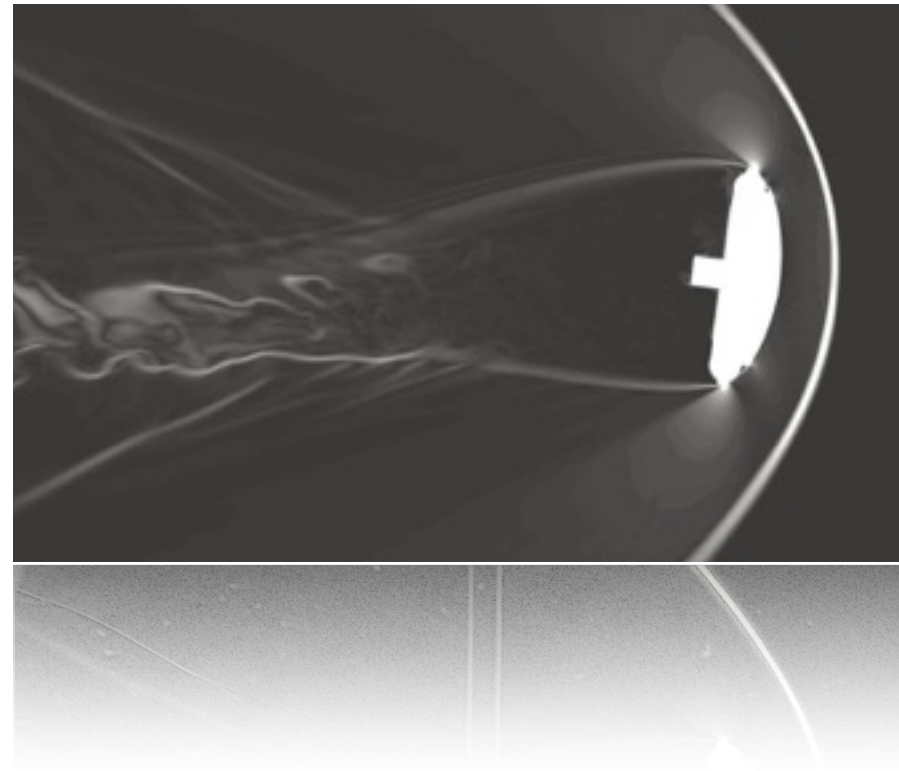


Simulated and Experimental Flow Field Comparison



- The simulation is initialized at static orientation of first experimental data point
 - This potentially misses vehicle-wake coupling at start up
- The simulation continues until the flow is converged to pseudo-steady state
 - Unsteady fluctuations of wake is statistically converged
- Comparison of density gradient magnitude from the simulation to shadowgraph images of the experiment show excellent qualitative agreement of dominant features

Shot	Mach
2623	2.03

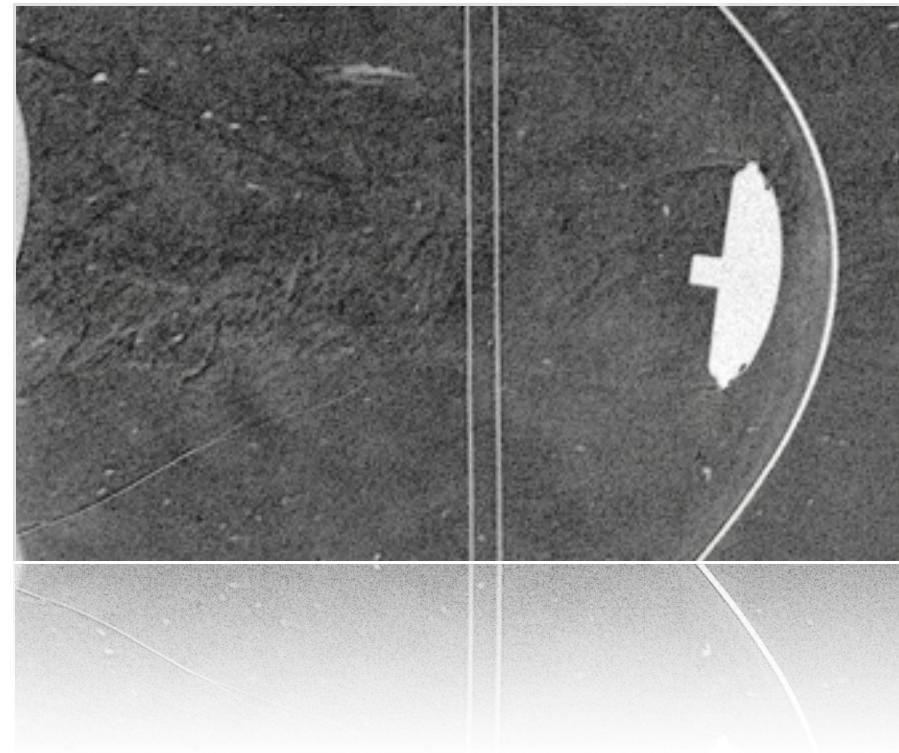


Simulated and Experimental Flow Field Comparison



- The simulation is initialized at static orientation of first experimental data point
 - This potentially misses vehicle-wake coupling at start up
- The simulation continues until the flow is converged to pseudo-steady state
 - Unsteady fluctuations of wake is statistically converged
- Comparison of density gradient magnitude from the simulation to shadowgraph images of the experiment show excellent qualitative agreement of dominant features

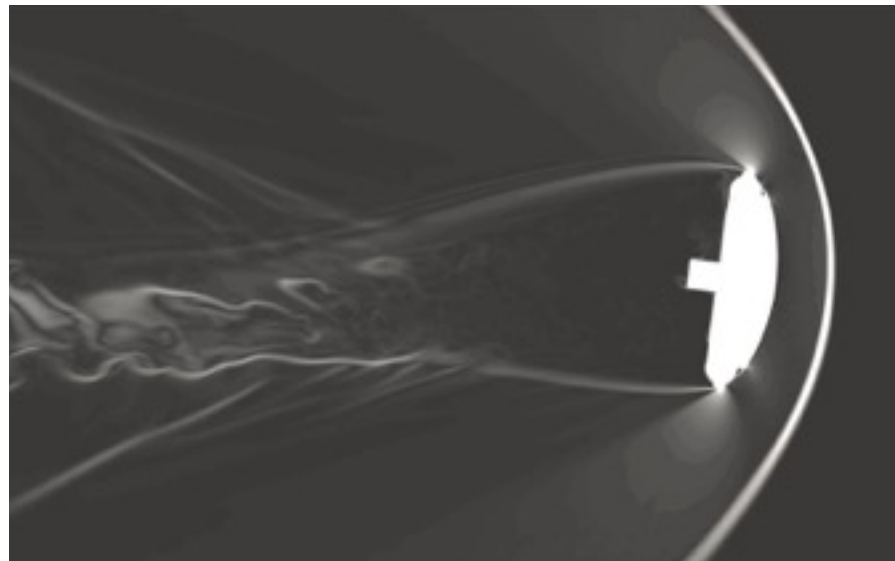
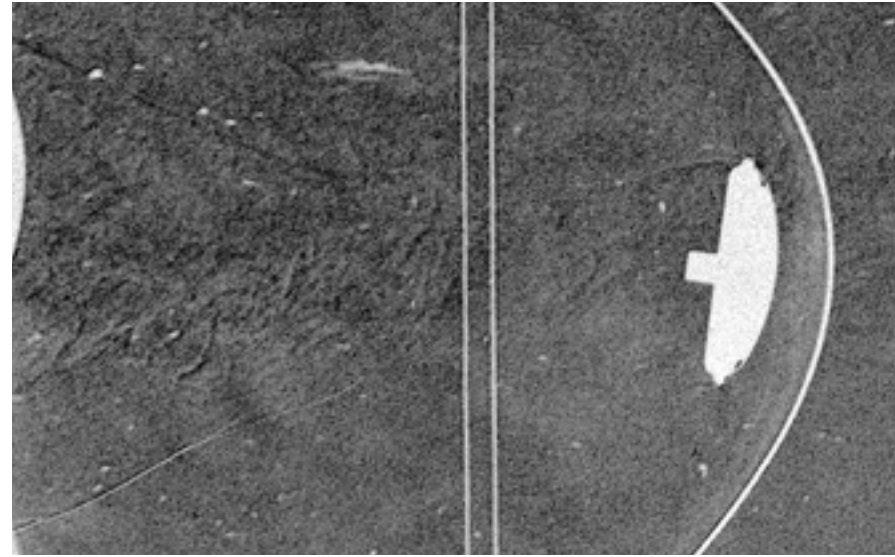
Shot	Mach
2623	2.03



Simulated and Experimental Flow Field Comparison



- The simulation is initialized at static orientation of first experimental data point
 - This potentially misses vehicle-wake coupling at start up
- The simulation continues until the flow is converged to pseudo-steady state
 - Unsteady fluctuations of wake is statistically converged
- Comparison of density gradient magnitude from the simulation to shadowgraph images of the experiment show excellent qualitative agreement of dominant features

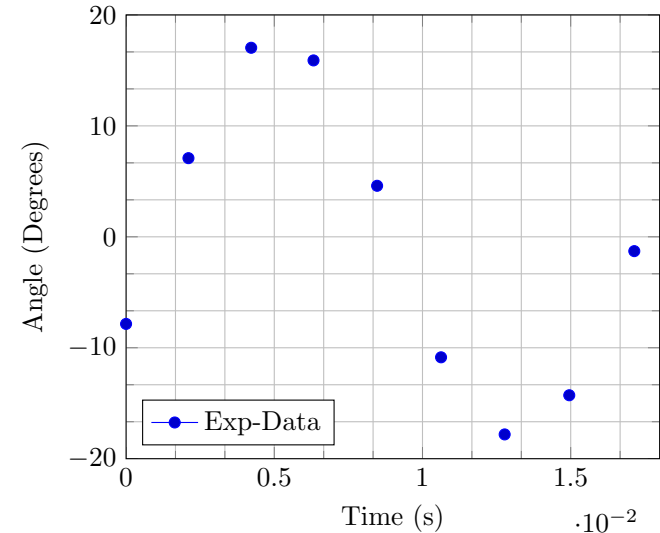


Dynamic Simulation Startup

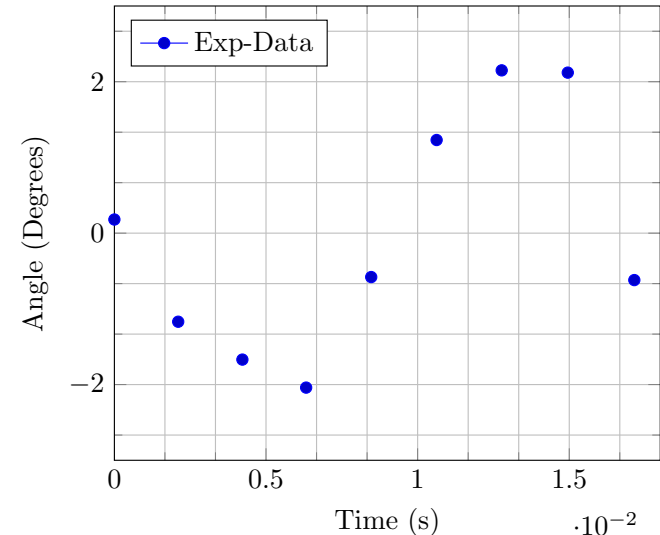


- Initial rates are taken from experimental data and applied to geometry
 - Fitted with cosine function and taking the first derivative of the function near the starting point
 - Derivative will be applied as a rotation rate to the mesh deformation
 - Some fits are poor due to rapid growth in oscillation of experiment or potential error in measured angle
 - Typically seen for small angles
 - Poor rate fits are instead approximated using linear derivative evaluation between first and second data point
 - Potential source of error if first or second experimental data point is significantly off

Pitch and Functional Fit vs. Time



Yaw and Functional Fit vs. Time

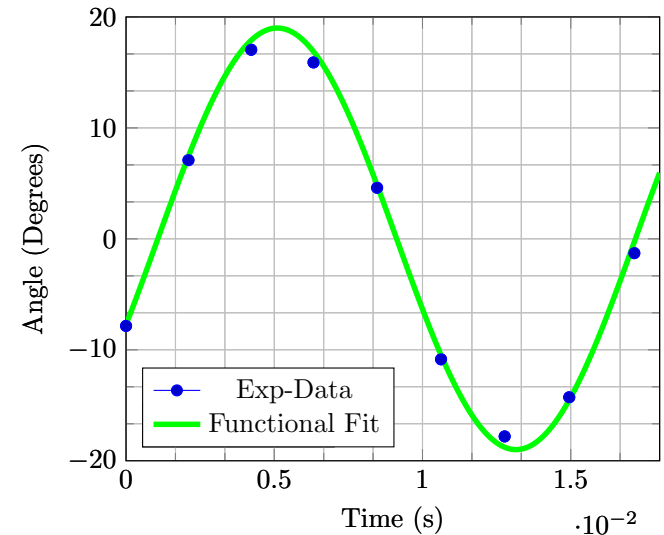


Dynamic Simulation Startup

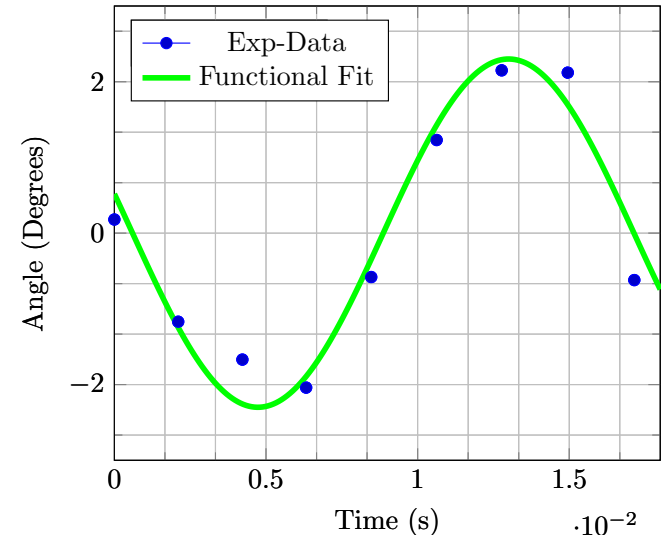


- Initial rates are taken from experimental data and applied to geometry
 - Fitted with cosine function and taking the first derivative of the function near the starting point
 - Derivative will be applied as a rotation rate to the mesh deformation
 - Some fits are poor due to rapid growth in oscillation of experiment or potential error in measured angle
 - Typically seen for small angles
 - Poor rate fits are instead approximated using linear derivative evaluation between first and second data point
 - Potential source of error if first or second experimental data point is significantly off

Pitch and Functional Fit vs. Time



Yaw and Functional Fit vs. Time

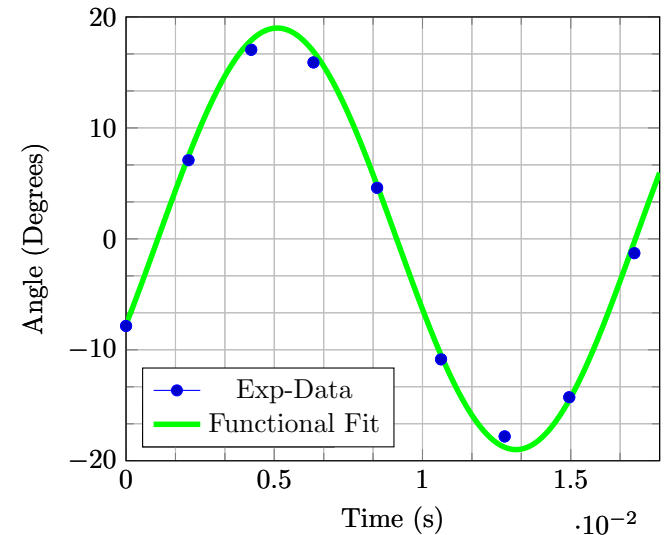


Dynamic Simulation Startup

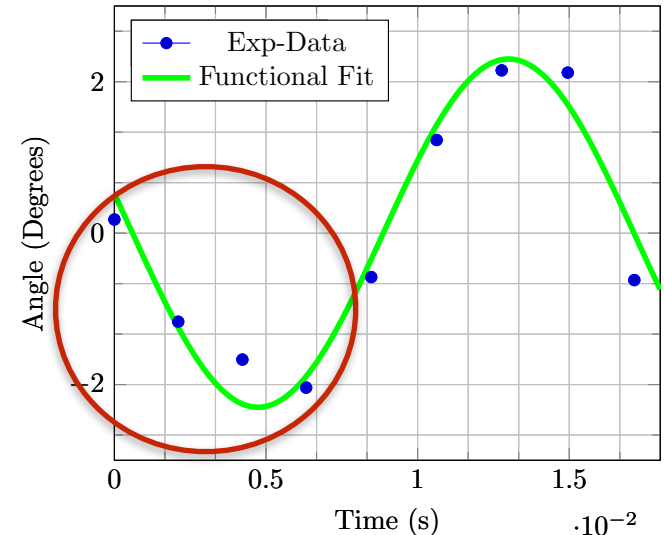


- Initial rates are taken from experimental data and applied to geometry
 - Fitted with cosine function and taking the first derivative of the function near the starting point
 - Derivative will be applied as a rotation rate to the mesh deformation
 - Some fits are poor due to rapid growth in oscillation of experiment or potential error in measured angle
 - Typically seen for small angles
 - Poor rate fits are instead approximated using linear derivative evaluation between first and second data point
 - Potential source of error if first or second experimental data point is significantly off

Pitch and Functional Fit vs. Time



Yaw and Functional Fit vs. Time



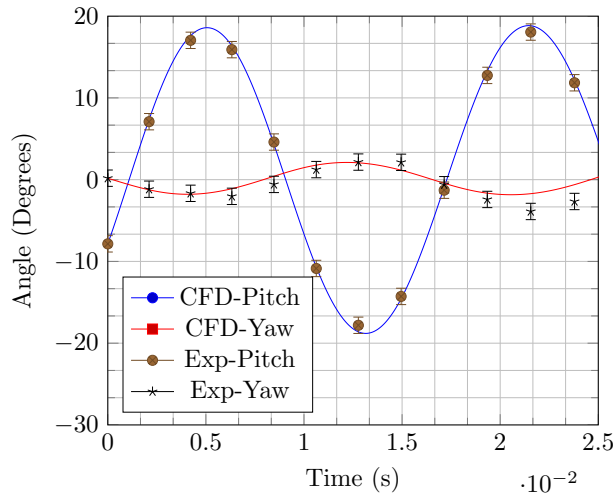
Dynamic Data Comparisons



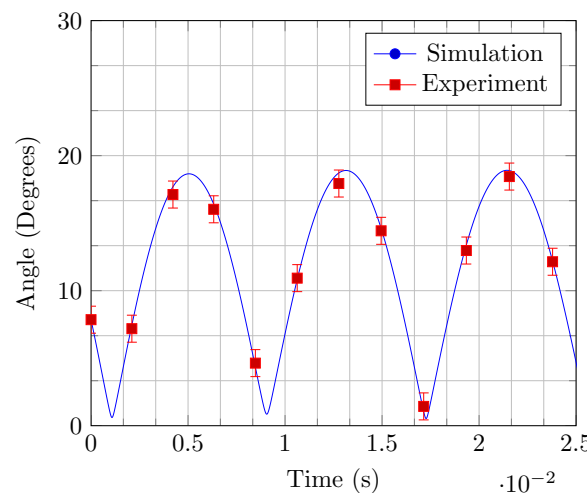
Shot	Mach
2623	2.03

$$\alpha_T = \cos^{-1} (\cos(\alpha) \cos(\beta))$$

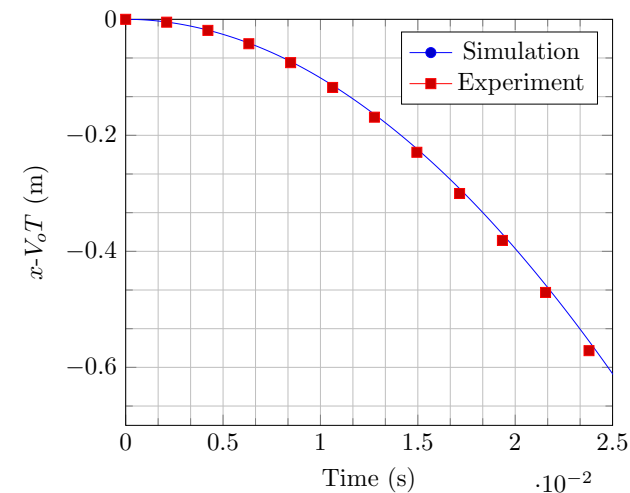
Pitch and Yaw vs. Time



Total Angle-of-Attack vs. Time



$x-V_oT$ vs Time



- Simulation data for pitch, yaw, total angle of attack and downstream distance is compared against experimental data
 - Experimental data assumed to have +/- 1° error
 - Oscillation amplitude and frequency of simulation matches very well against experiment
 - Predicted downstream distance shows excellent agreement with experimental data
 - Indicating good agreement in drag

Dynamic Data Comparisons



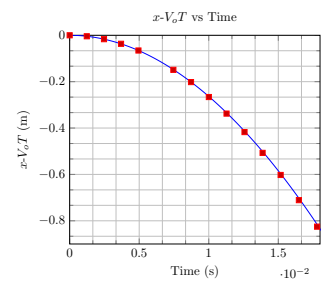
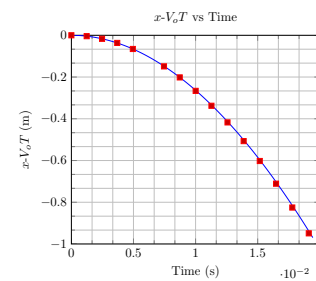
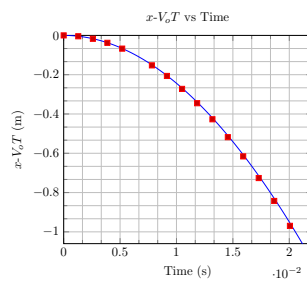
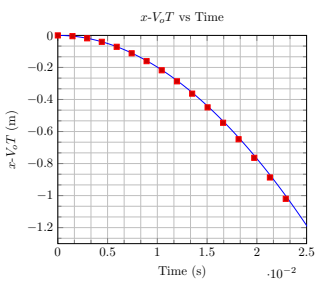
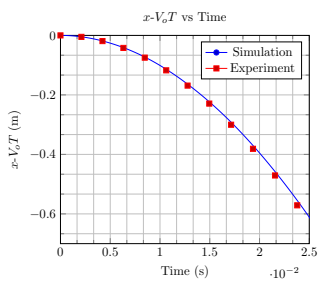
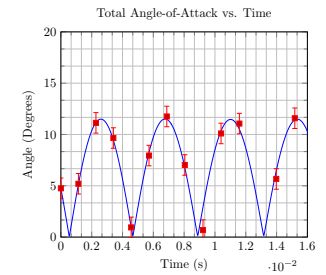
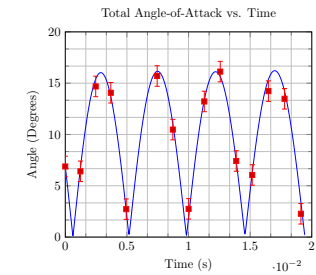
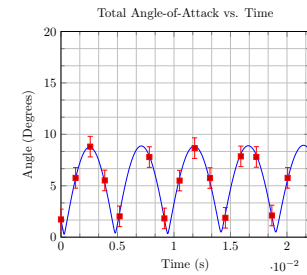
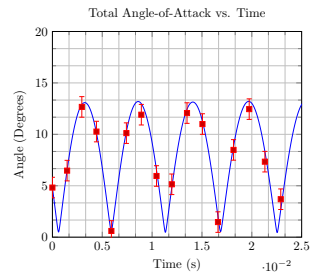
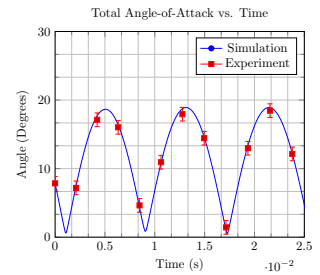
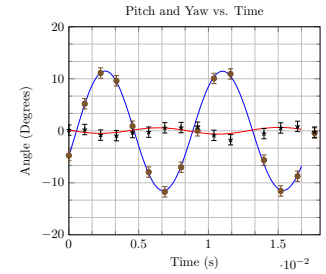
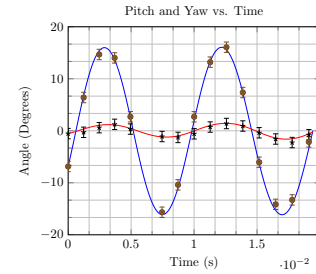
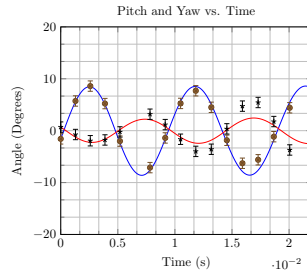
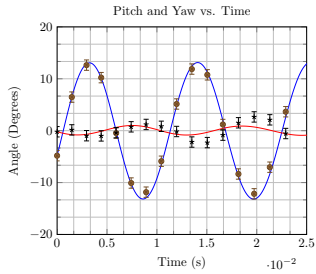
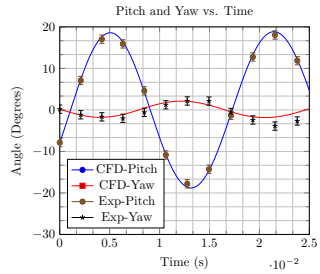
Shot	Mach
2623	2.03

Shot	Mach
2642	2.91

Shot	Mach
2643	3.31

Shot	Mach
2648	3.49

Shot	Mach
2638	3.78



Excellent agreement with raw experimental data. How well do derived aerodynamic coefficients compare?

CADRA Analysis



- Trajectories are reduced to aerodynamic coefficients using the Comprehensive Aerodynamic Data Reduction System for Aeroballistic Ranges (CADRA2) program
- CADRA calculates trajectory of the ballistic range model by integrating twelve coupled first-order differential equations of motion in earth- and body-fixed coordinate systems
- Aerodynamic coefficients are modeled as nonlinear series

$$C_X = \sum_{m=1}^{m-\max} [C_{X_{mn}} + (M - M_{ref})^m] \sin^n \alpha$$

CFD data contains ~150,000 points per trajectory, which is down sampled to 16 for a one-to-one comparison to experimental data.

CADRA Analysis



- Trajectories are reduced to aerodynamic coefficients using the Comprehensive Aerodynamic Data Reduction System for Aeroballistic Ranges (CADRA2) program
- CADRA calculates trajectory of the ballistic range model by integrating twelve coupled first-order differential equations of motion in earth- and body-fixed coordinate systems
- Aerodynamic coefficients are modeled as nonlinear series

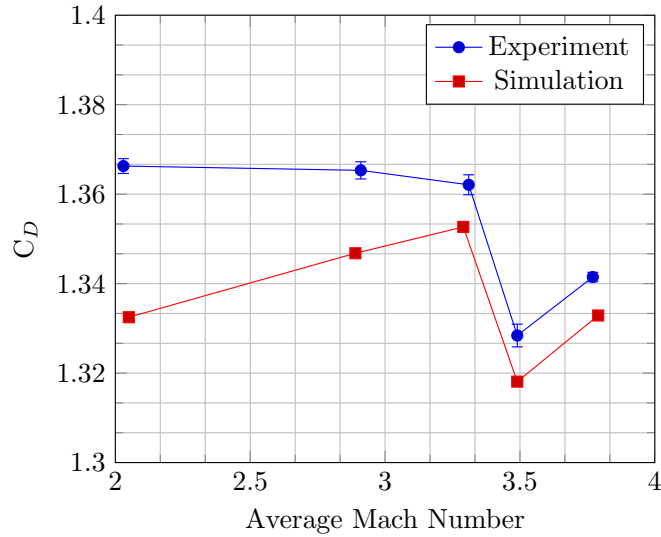
$$\begin{aligned} C_D = & \left[C_{D_0} + C_{D_{(M-M_{ref})}} (M - M_{ref}) + C_{D_{(M-M_{ref})^2}} (M - M_{ref})^2 \right] \sin \alpha \\ & + \left[C_{D_{\alpha^2}} + C_{D_{\alpha^2, (M-M_{ref})}} (M - M_{ref}) + C_{D_{\alpha^2, (M-M_{ref})^2}} (M - M_{ref})^2 \right] \sin^2 \alpha \\ & + \left[C_{D_{\alpha^4}} + C_{D_{\alpha^4, (M-M_{ref})}} (M - M_{ref}) + C_{D_{\alpha^4, (M-M_{ref})^2}} (M - M_{ref})^2 \right] \sin^4 \alpha \end{aligned}$$

CFD data contains ~150,000 points per trajectory, which is down sampled to 16 for a one-to-one comparison to experimental data.

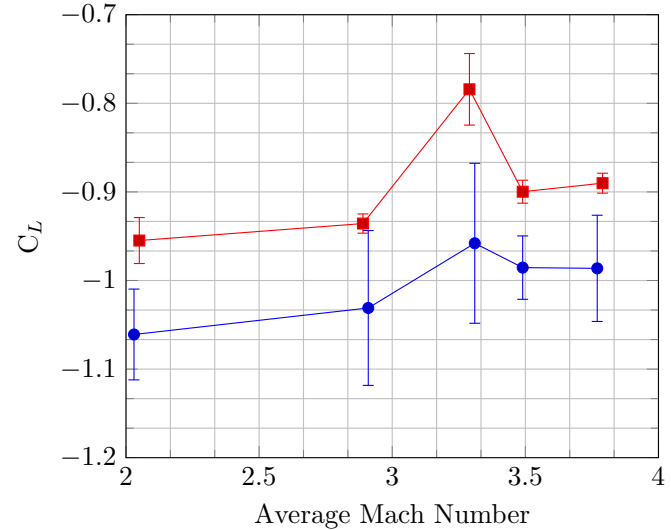
CADRA2 Derived Dynamic Coefficients



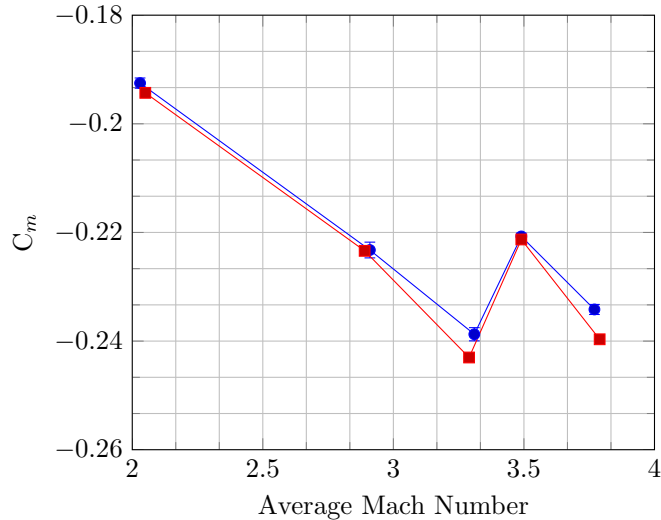
Drag Coefficient



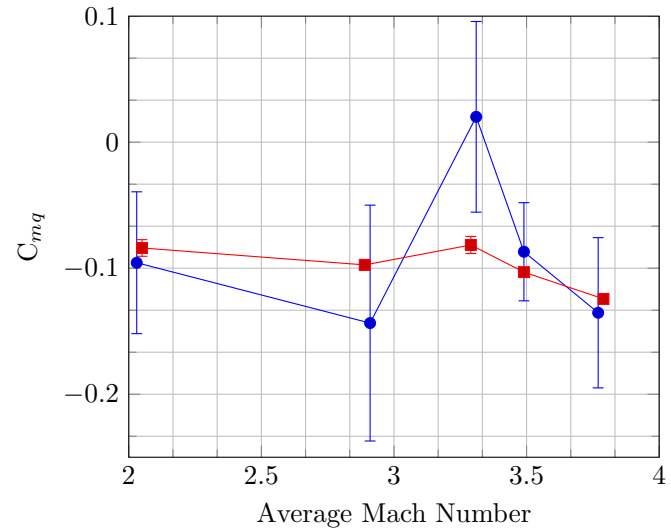
Lift Coefficient



Moment Coefficient



Pitch Damping Coefficient

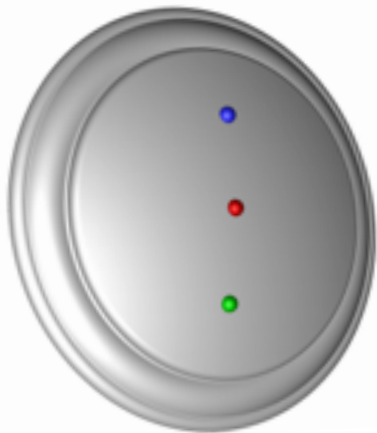


Investigation of Flow Physics



- An advantage of CFD is the capability of probing flow physics at various regions for minimal to no additional cost
- Several pressure probes placed were on vehicle surface and in near wake of vehicle
- Time history data of pressure coefficient shows lag in wake pressure response compared to forebody
 - Lag has been previously stated as a mechanism of instability by Teramoto *et al.* [6,7]

Shot	Mach
2623	2.03

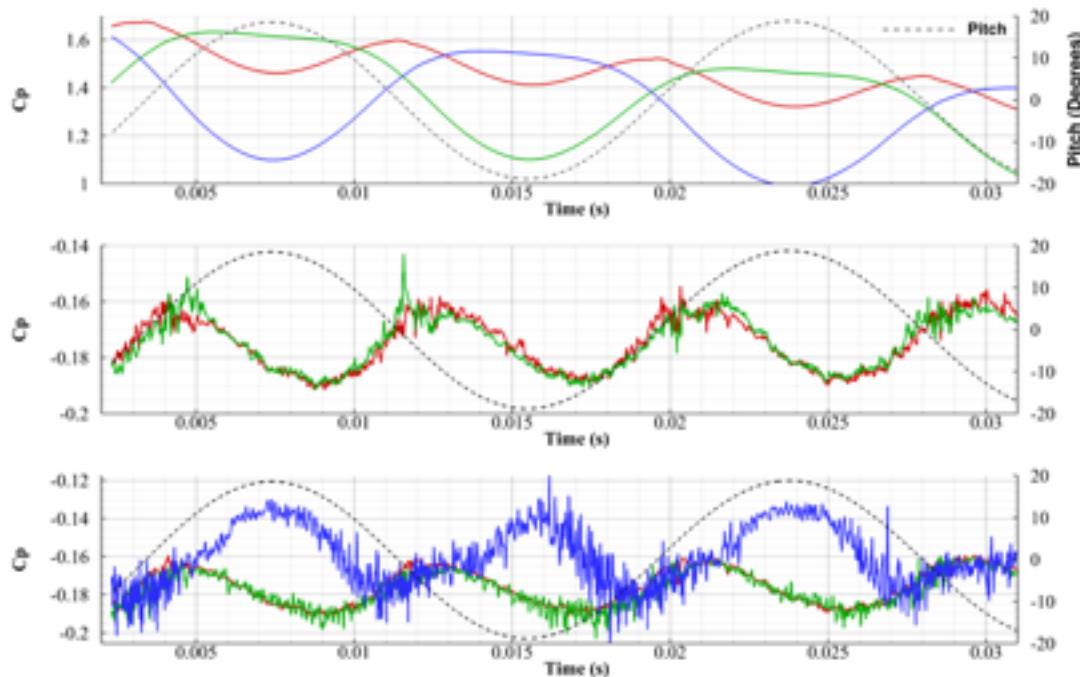


Investigation of Flow Physics



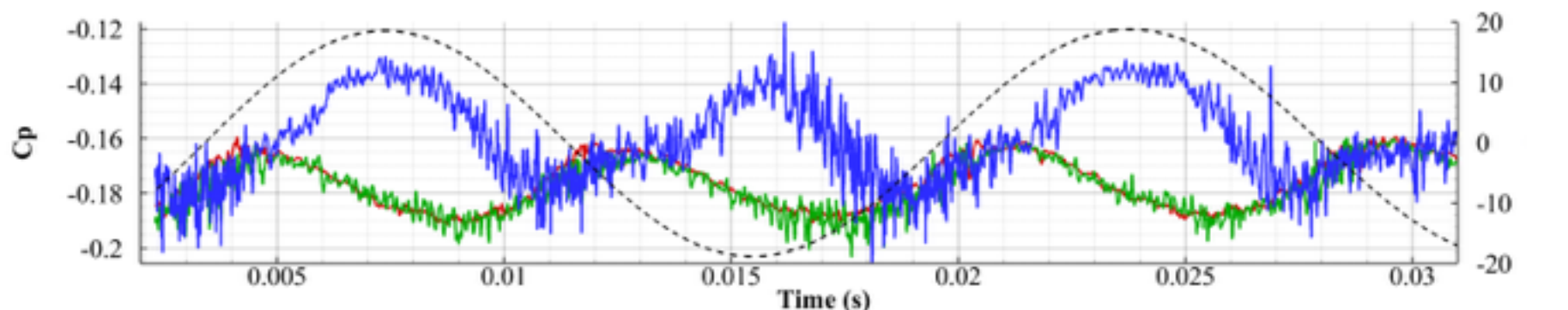
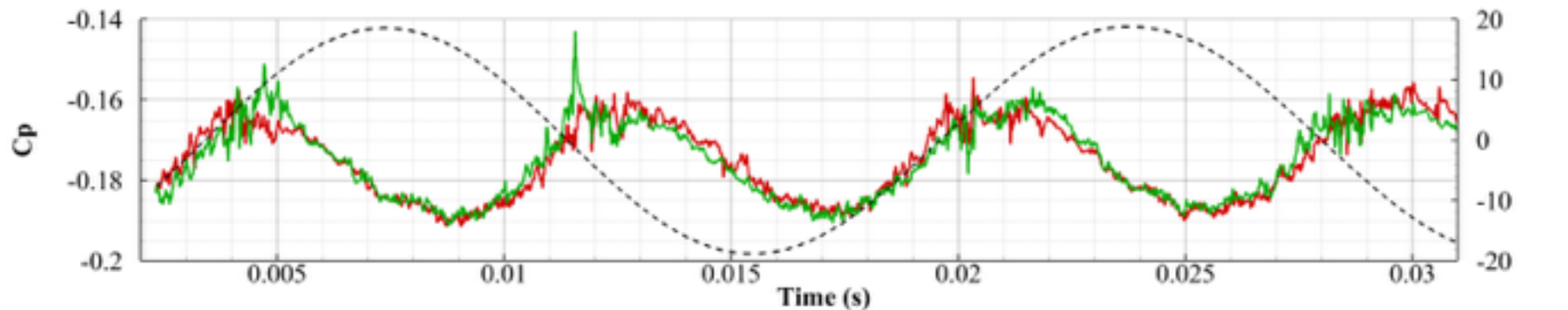
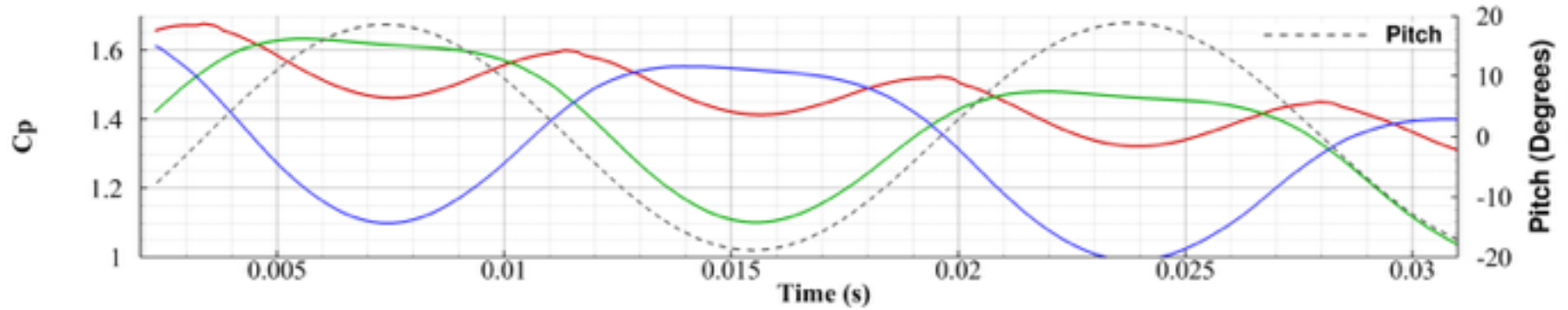
- An advantage of CFD is the capability of probing flow physics at various regions for minimal to no additional cost
- Several pressure probes placed were on vehicle surface and in near wake of vehicle
- Time history data of pressure coefficient shows lag in wake pressure response compared to forebody
 - Lag has been previously stated as a mechanism of instability by Teramoto *et al.* [6,7]

Shot	Mach
2623	2.03

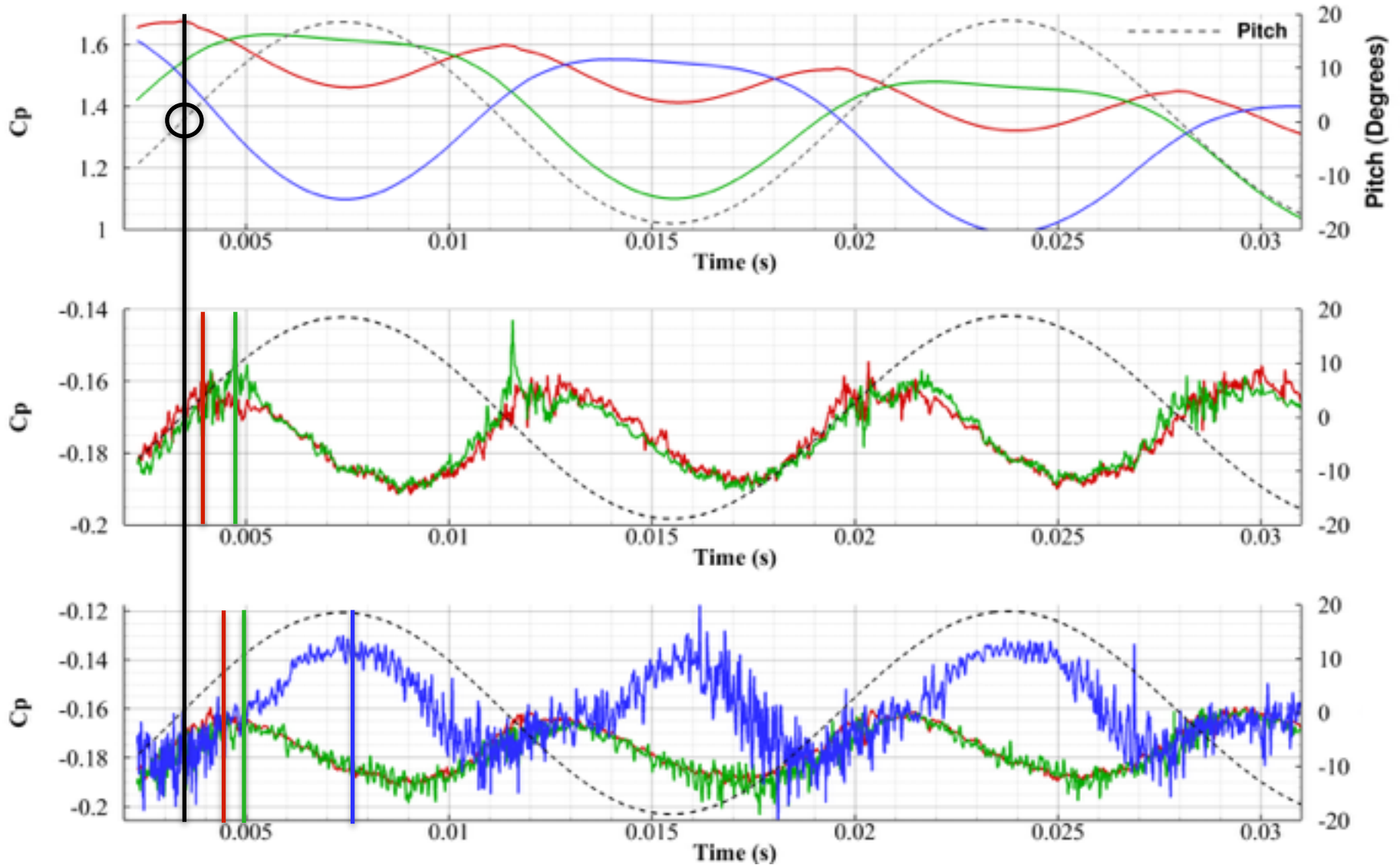




Investigation of Flow Physics

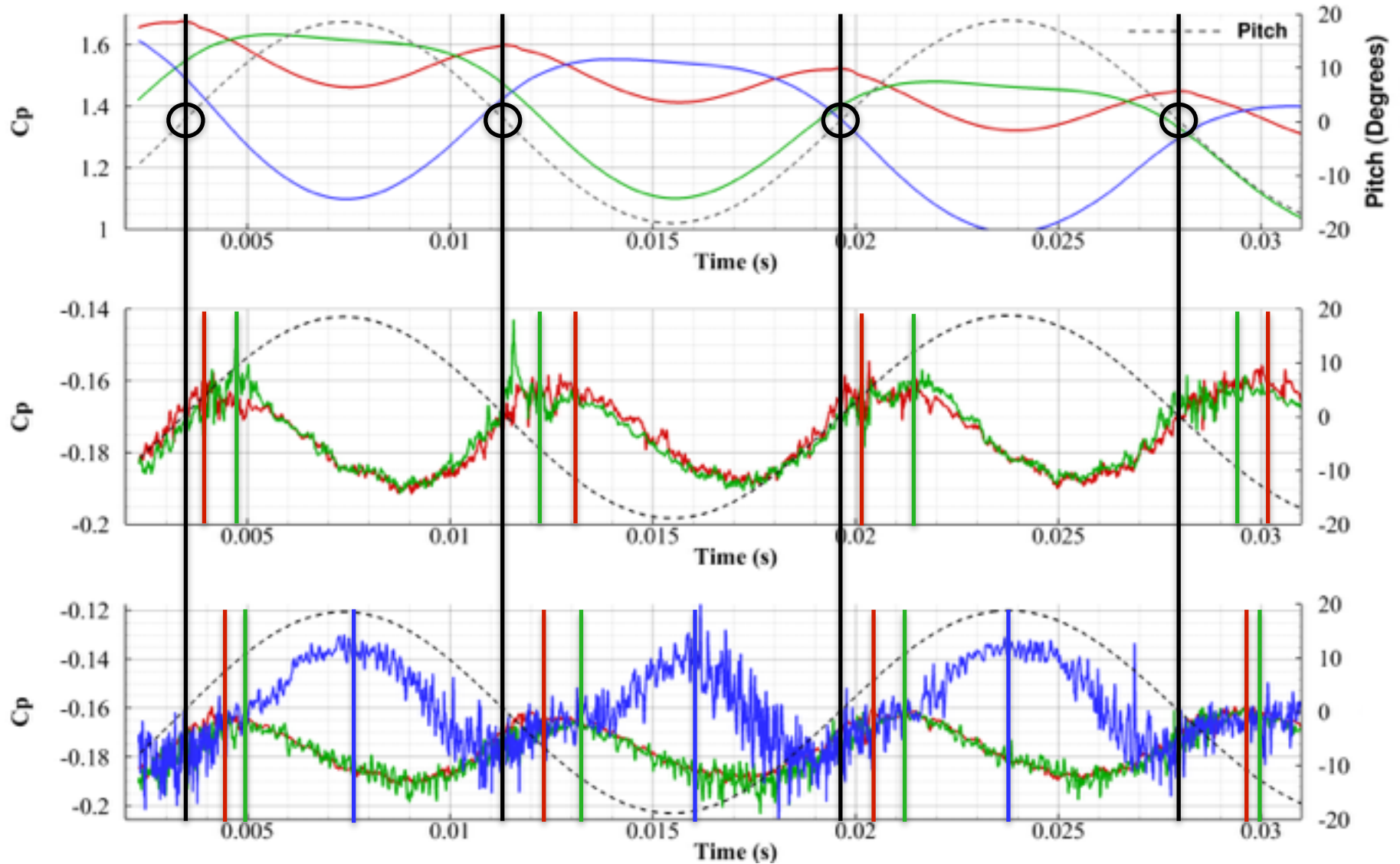


Investigation of Flow Physics





Investigation of Flow Physics

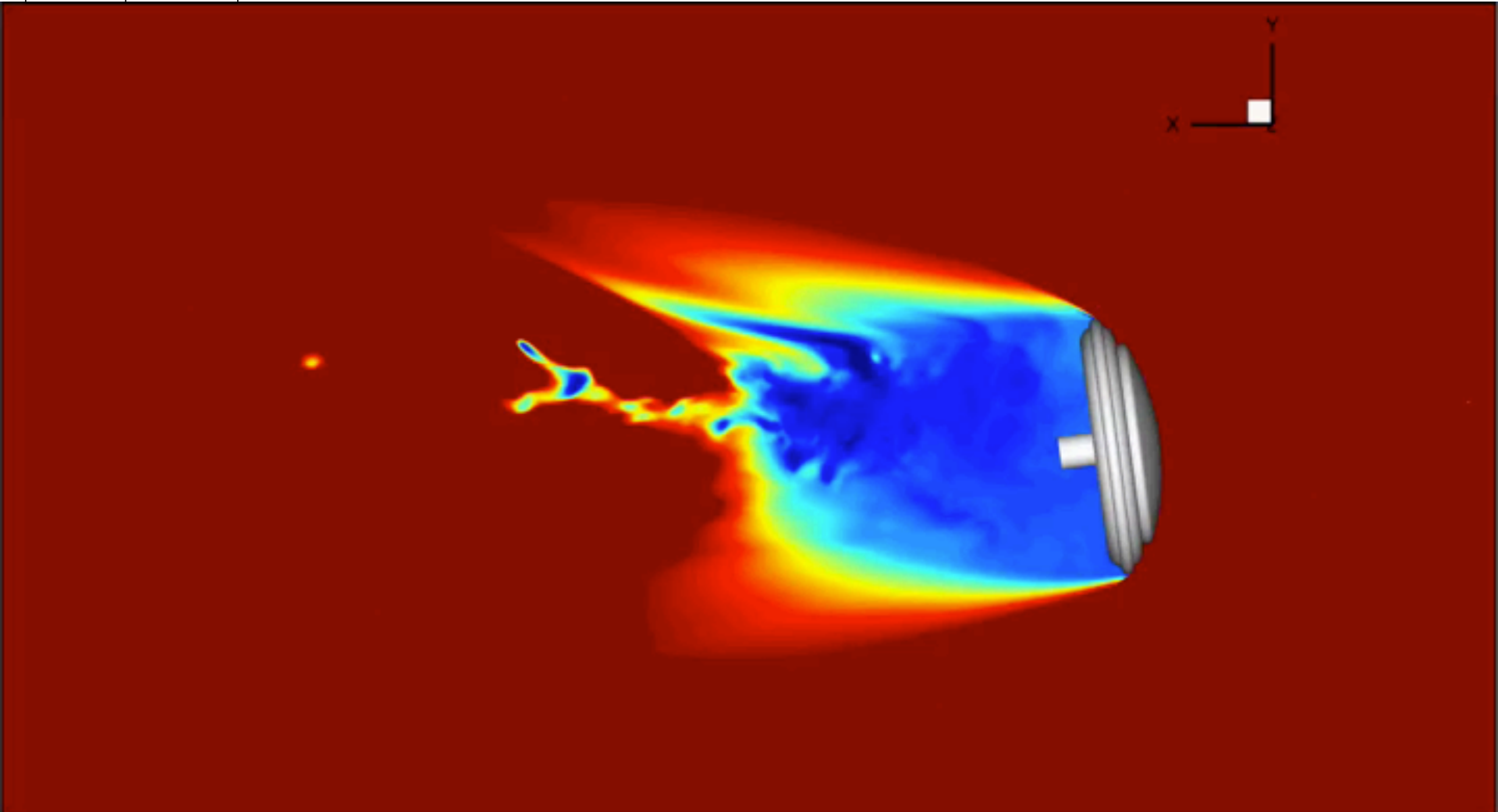




Wake Flow Pressure



Shot	Mach
2623	2.03

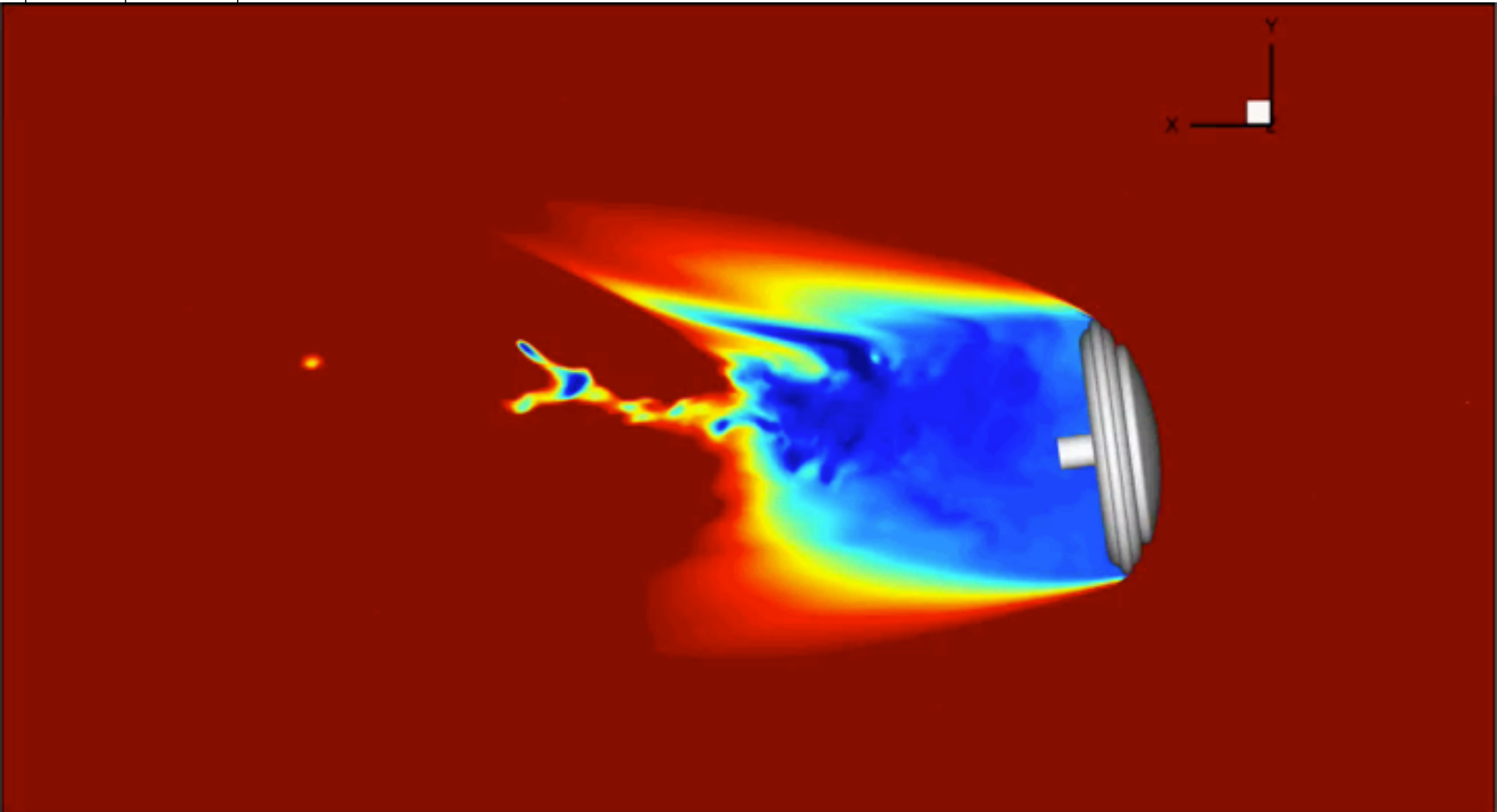




Wake Flow Pressure



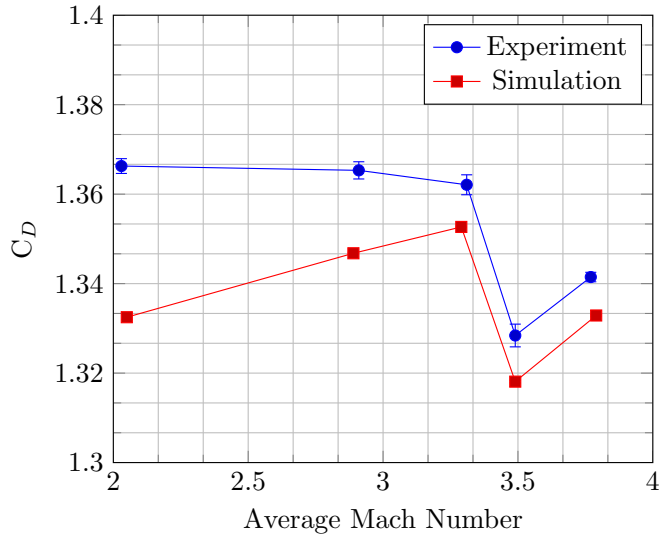
Shot	Mach
2623	2.03



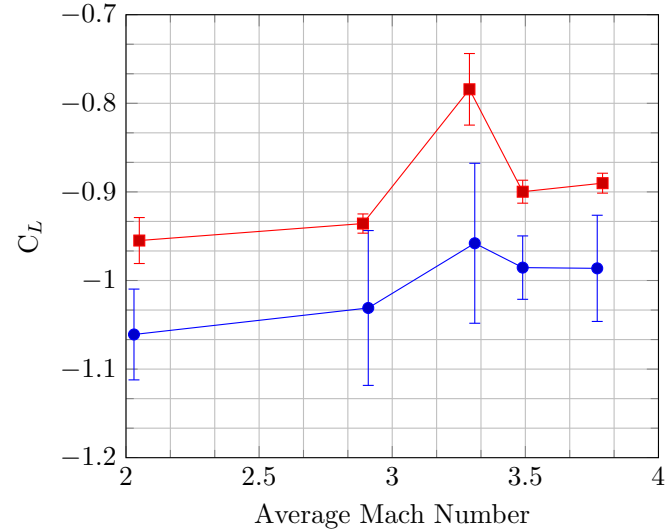
CADRA2 Derived Dynamic Coefficients



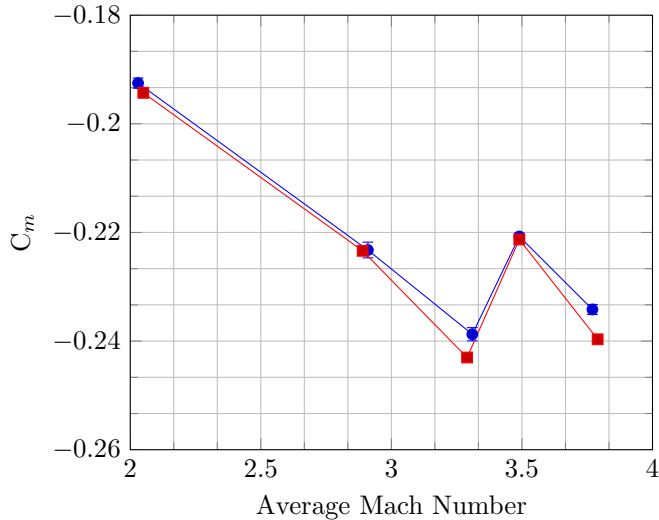
Drag Coefficient



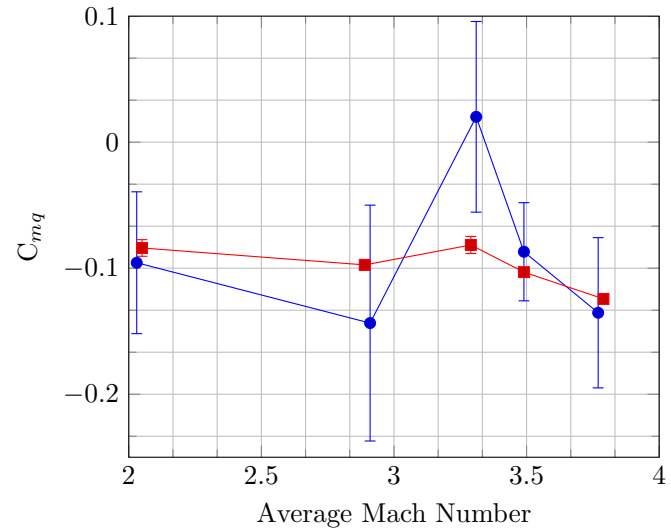
Lift Coefficient



Moment Coefficient



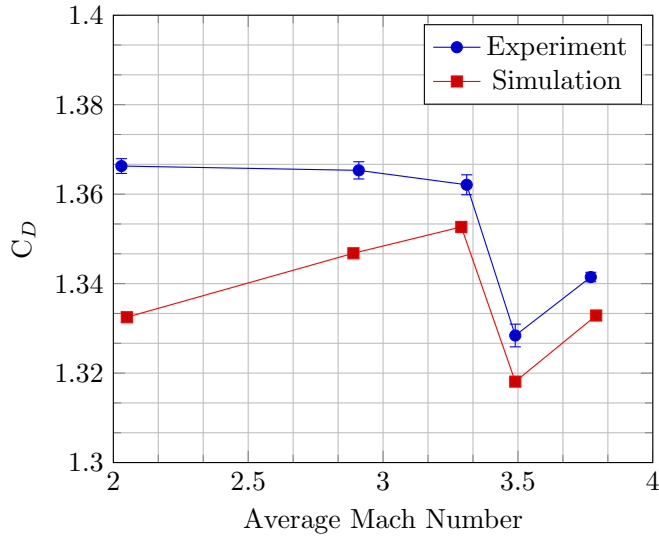
Pitch Damping Coefficient



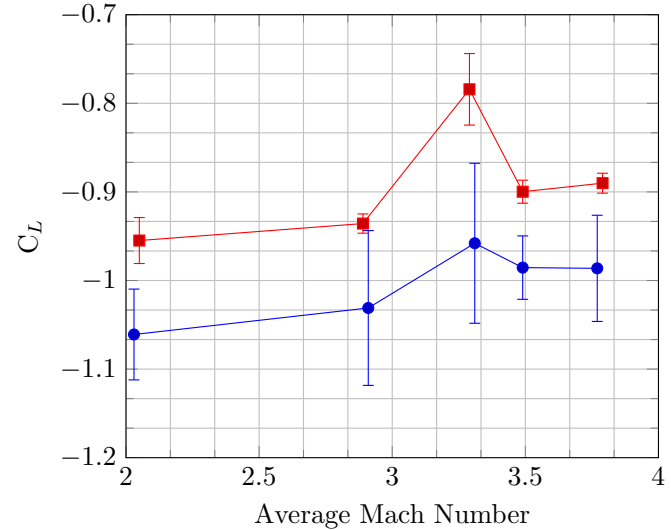
CADRA2 Derived Dynamic Coefficients



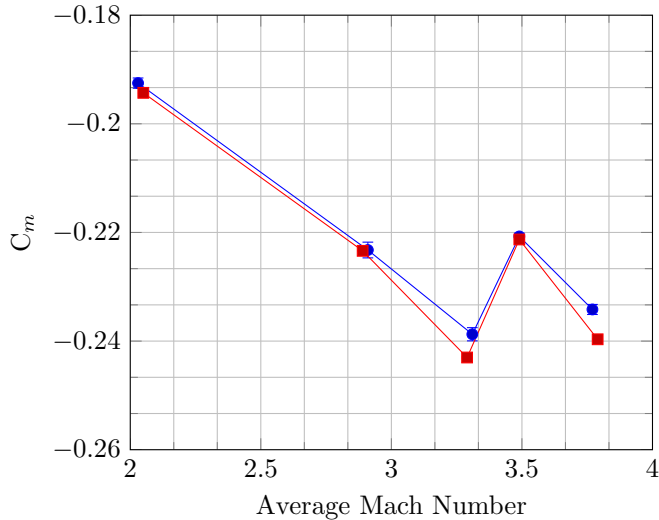
Drag Coefficient



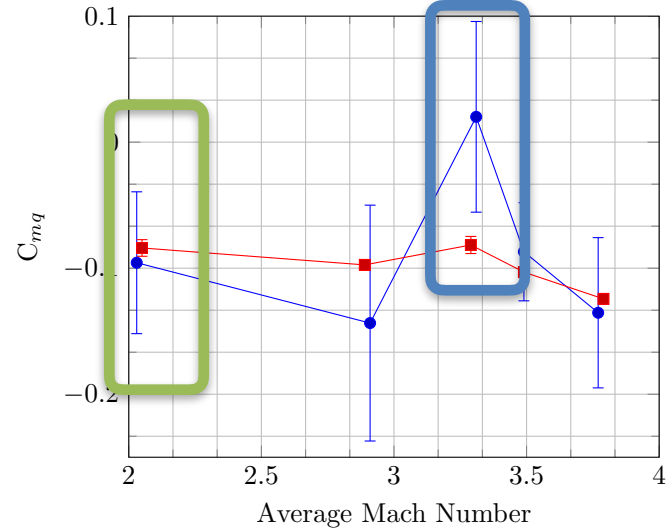
Lift Coefficient



Moment Coefficient



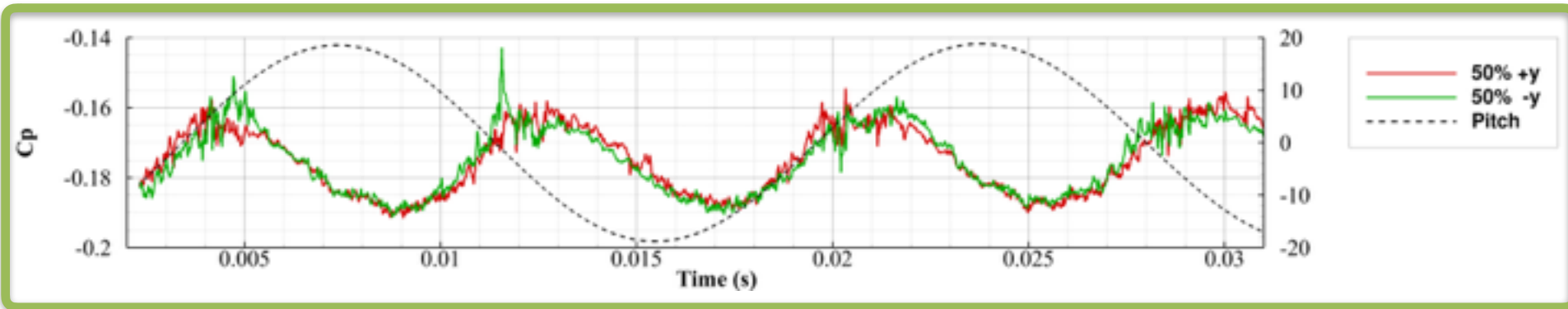
Pitch Damping Coefficient



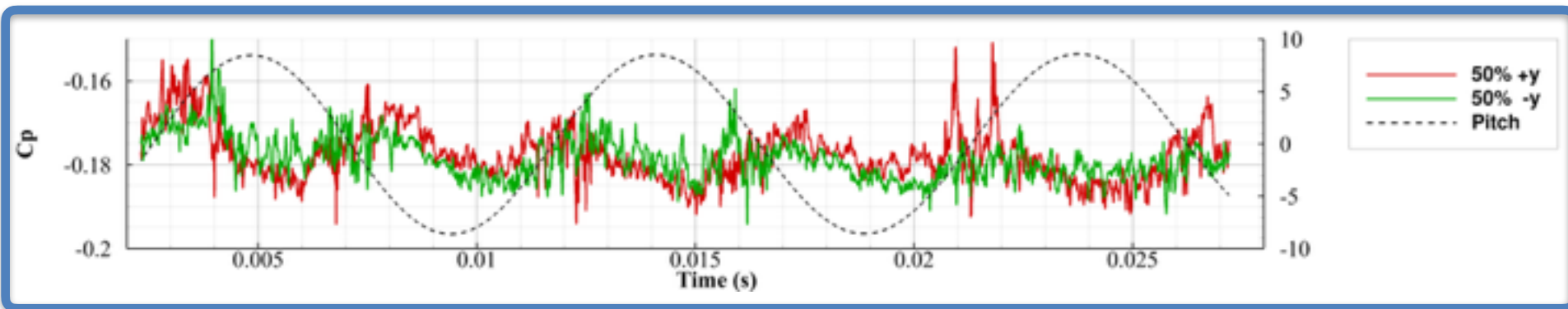
CADRA2 Derived Dynamic Coefficients



Shot	Mach
2623	2.03



Shot	Mach
2643	3.31

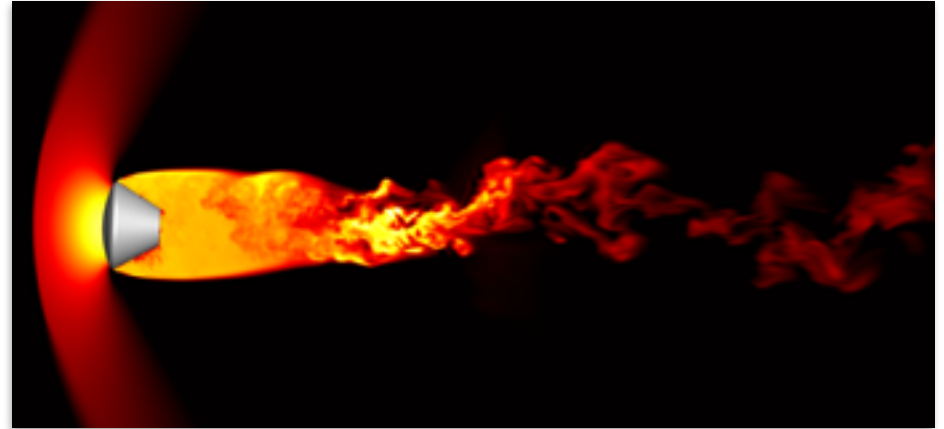
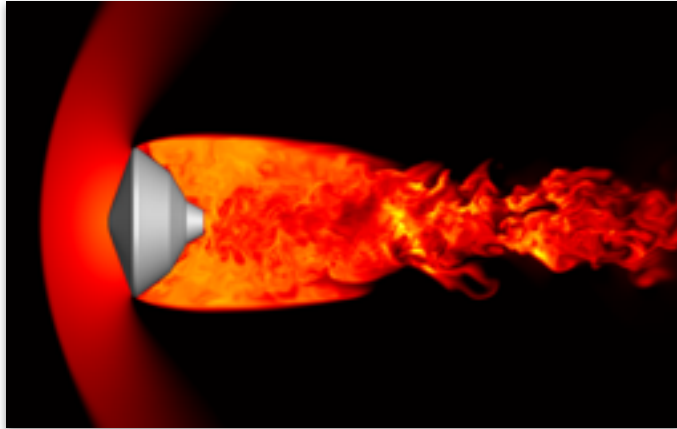


Summary/Conclusions



- Free-flight CFD simulations of a ballistic range model based on the SFDT vehicle architecture have been performed using US3D
- Results based on artificial start-up methodology produces excellent agreement in vehicle attitude to raw experimental pitch and yaw data
- Derived aerodynamic coefficients using the NASA code CADRA for the simulation results and experimental data were compared
 - Overall trends match quite well for all variables with disagreements mainly in the lift and low Mach number drag
 - Simulation moment coefficient agreed well with experimental data
 - Pitch damping coefficient comparison showed similar trends except for the Mach 3.31 data point
- The ability to probe flow physics from the CFD was used to investigate fluid dynamic coupling
 - Forebody and aftbody pressure fields in response to vehicle attitude suggest coupling Wake probes suggest pressure waves travel downstream
 - A result that is contrary to earlier findings

Future Work



Stern et al. (upcoming)

- Continue validation/verification of US3D as a computational tool to predict dynamic stability within supersonic regime
 - Investigate startup conditions and their consequences on long-time dynamic behavior
 - Compare flight scale simulation against reconstructed flight data
 - Further investigate physical mechanisms
- Wider range of supersonic cases and geometries will be considered
- Further validation/verification within the subsonic-transonic regime will be sought

Acknowledgements



- Michael Barnhardt
- Cole Kazemba
- Entry Systems Modeling (ESM) project within NASA's Game Changing Development Program
- AMA Inc. under contract NASA NNA15BB15C



Questions?



References



1. Bowes, Angela L., et al. "LDSO POST2 Simulation and SFDT-1 Pre-Flight Launch Operations Analyses." (2015).
2. Brown, Jeffrey D., et al. "Transonic Aerodynamics of a Lifting Orion Crew Capsule from Ballistic Range Data." *Journal of Spacecraft and Rockets* 47.1 (2010): 36-47.
3. Murman, Scott M. "Dynamic simulations of atmospheric-entry capsules." *Journal of Spacecraft and Rockets* 46.4 (2009): 829-835.
4. Stern, Eric, Vladimir Gidzak, and Graham V. Candler. "Estimation of Dynamic Stability Coefficients for Aerodynamic Decelerators Using CFD." *AIAA Applied Aerodynamics Conference*, New Orleans, LA. 2012.
5. Nompelis, Ioannis, Travis W. Drayna, and Graham V. Candler. "Development of a hybrid unstructured implicit solver for the simulation of reacting flows over complex geometries." *AIAA Paper* 2227 (2004): 2004.
6. Nompelis, Ioannis, Travis W. Drayna, and Graham V. Candler. "A parallel unstructured implicit solver for hypersonic reacting flow simulation." *17 th AIAA Computational Flow Dynamics Conference*. 2005.
7. Teramoto, Susumu, Kouju Hiraki, and Kozo Fujii. "Numerical analysis of dynamic stability of a reentry capsule at transonic speeds." *AIAA journal* 39.4 (2001): 646-653.
8. Teramoto, Susumu, and Kozo Fujii. "Mechanism of dynamic instability of a reentry capsule at transonic speeds." *AIAA journal* 40.12 (2002): 2467-2475.
9. Subbareddy, Pramod K., and Graham V. Candler. "A fully discrete, kinetic energy consistent finite-volume scheme for compressible flows." *Journal of Computational Physics* 228.5 (2009): 1347-1364.
10. Spalart, Philippe R., and Steven R. Allmaras. "A one equation turbulence model for aerodynamic flows." *AIAA journal* 94 (1992).
11. Spalart, P. R., et al. "Comments on the feasibility of LES for wings, and on a hybrid RANS/LES approach." *Advances in DNS/LES* 1 (1997): 4-8.
12. GridPro, "az3000", Ver.4.3 and Program Development Co. and White Plains, NY, 2008



Backup



US3D Flow Solver

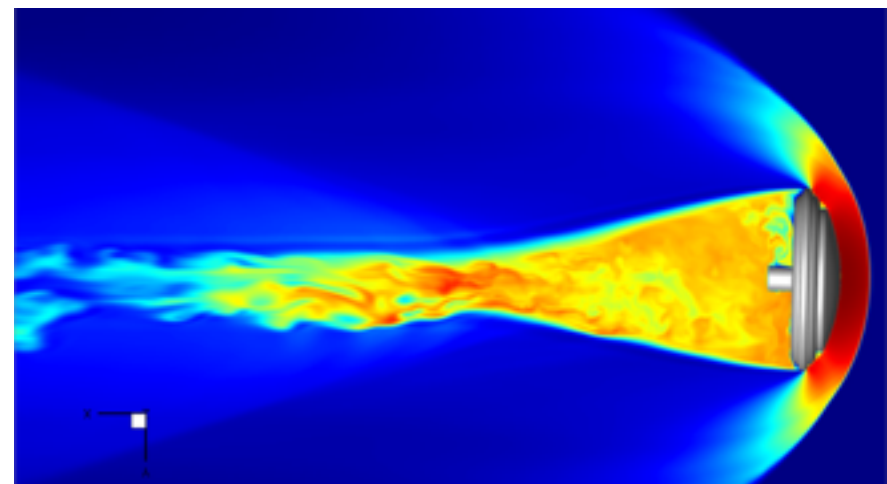
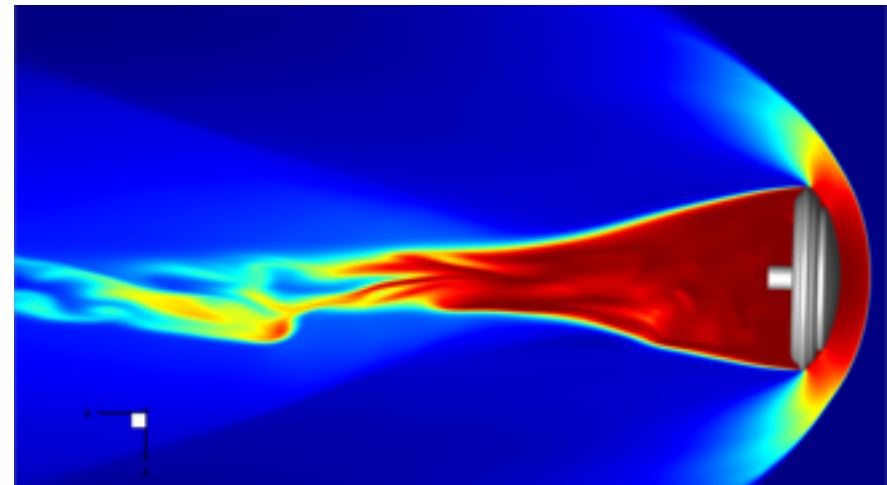


- Developed at the University of Minnesota by Graham Candler and students
- 3-dimensional parallel unstructured cell-centered finite-volume Navier-Stokes solver
 - Ability to solve on structured, unstructured, and hybrid grid topologies
 - Spatial fluxes can be;
 - 2nd and 3rd order upwind fluxes
 - 2nd, 4th, and 6th order Kinetic Energy Consistent (KEC)[5] low-dissipation fluxes
 - Time integration achieved through 3rd order explicit (RK3), or second order implicit (DPLR and FMPR) schemes
 - Finite Rate chemistry and vibrational-electronic energy relaxation
 - Turbulence modeling available through;
 - Algebraic Baldwin Lomax model
 - One equation Spalart Almaras model [6]
 - Shear-Stress-Transport (SST) k-omega model
 - Wall model LES implemented using DES97, DDES, IDDES [7]
 - Mesh motion capability to perform dynamic simulations

Importance of Numerical Accuracy



- The CFD solver used for all simulations presented was US3D [2,3]
 - US3D offers the capability of handling complex structured/unstructured mesh types
 - Additional advantage comes in the form of a low-dissipation spatial flux scheme which is crucial in resolving wake flows
- Upwind schemes are inherently dissipative
 - Too much dissipation results in attenuation of small scale structures and diffuses strong gradients
- Large amounts of dissipation truncates energy cascade, which increases dissipation length scale
 - Seen here as a temperature increase for upwind method

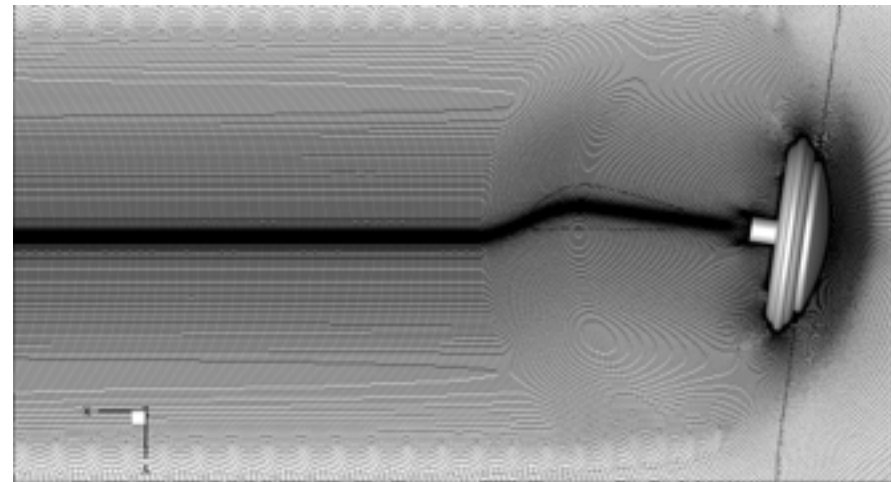
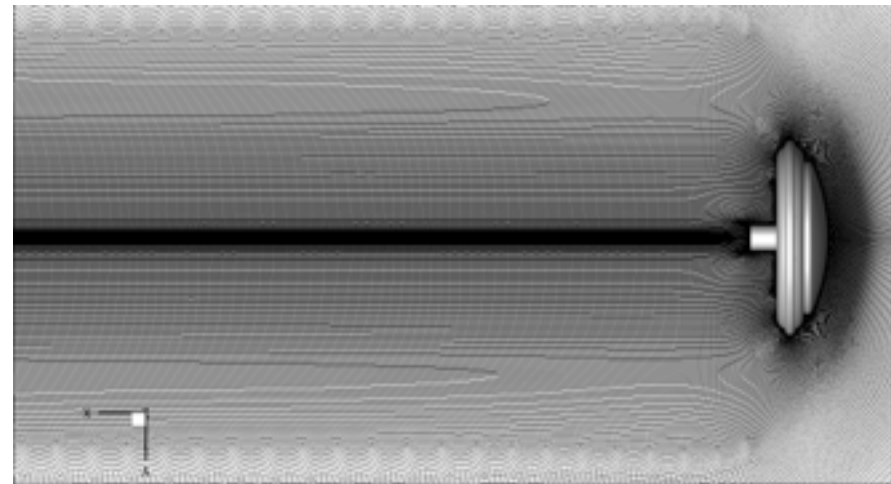




US3D Dynamic Solver



- Grid motion is achieved through deformation of the mesh
 - Mesh split into 3 regions
 - Near body mesh undergoes rigid body rotation
 - Intermediate region behaves as a sponge region to blend inner and outer regions
 - Outer region remains unchanged
- The mesh motion allows the vehicle to pitch, yaw, and rotate
 - 6-DOF motion is achieved through frame velocity changes applied to faces fluxes

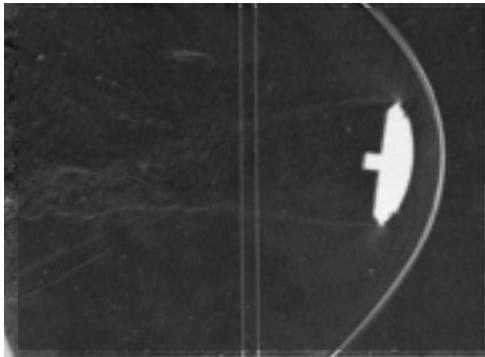




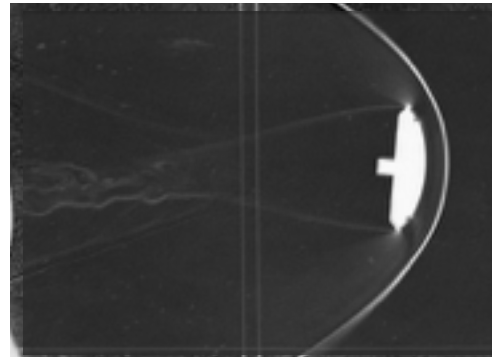
Shadowgraph Comparisons



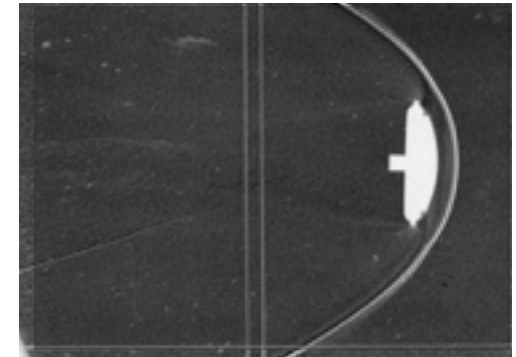
Run	Average Mach
Shot 2623	2.01



Run	Average Mach
Shot 2642	2.89



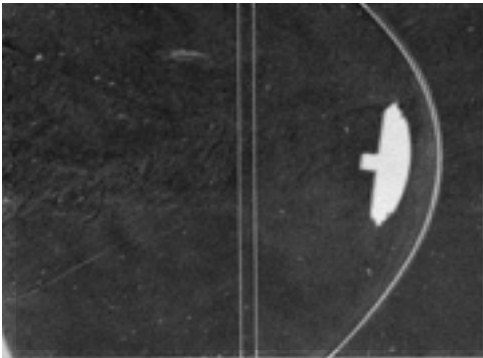
Run	Average Mach
Shot 2643	3.29



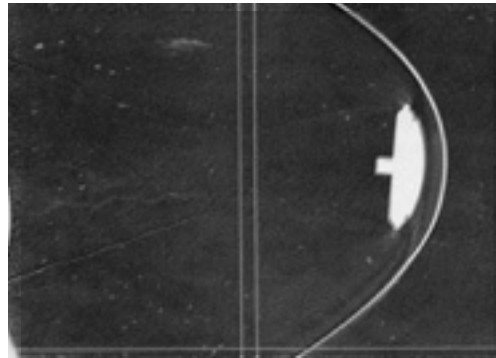
Shadowgraph Comparisons



Run	Average Mach
Shot 2623	2.01



Run	Average Mach
Shot 2642	2.89



Run	Average Mach
Shot 2643	3.29

